Università degli Studi di Palermo

INTERNATIONAL PhD COURSE IN IMMUNOPHARMACOLOGY

Dean:

Professor Francesco Dieli

Modulation of tumor phenotype by metastatic cancer exosomes

PhD Student:

Odessa Schillaci

Tutor:

Professor Simona Fontana

Ciclo XXVI – SSD MED/04- a.a. 2012-15

INDEX:

Abstract

Tumors are characterized by intratumoral heterogeneity that makes the development of new treatments difficult. Several studies suggest that exosomes may be an important microenvironmental factor affecting tumor heterogeneity. In this context our goal is to understand if exosomes derived from cell line with highly metastatic potential, may affect the behavior of less aggressive cells and the properties of tumor microenvironment.

Our experimental strategy is based on the use of an isogenic model. We used SW480 and SW620 colon carcinoma cell lines derived from, respectively, primary and secondary tumors resected from a single patient, thus showing different metastatic potential. Specifically we evaluated, at morphological and functional level, how exosomes derived from highly metastatic cells influence the biological behavior of both less aggressive and endothelial cells. Finally we performed a proteomic characterization of exosomes by SWATH-MS method.

We found that exosomes released by amoeboid SW620 cells are able to induce a mesenchymal-amoeboid transition in SW480 fibroblast-like cells. We observed that after treatment with SW620 exosomes, SW480 cells show non apoptotic membrane blebbing, associated with higher migratory and invasive capabilities. Moreover, the treatment of the HUVECs with SW620 exosomes induce the monolayer permeability, due to destabilization of endothelial junctional systems. Our data indicate that the effects of SW620 exosomes treatment is mediated by RhoA, responsible of cytoskeletal remodeling. Moreover, this data was strongly supported by quantitative proteomic analysis showing an enrichment in SW620 exosomes of RacGap1, activator of RhoA.

We demonstrated that, through exosomes, highly metastatic cells spread their malignant behavior to less aggressive cells and affect tumor microenvironment.

Introduction

Colorectal cancer: prevalence, aetiology and carcinogenesis

Colorectal cancer (CRC) is the second most frequent malignant disease in the developed countries. The highest incidence rates of CRC are seen in North America, Australia and Europe, and the lowest rates in Africa and Asia [1]. The incidence of CRC is higher for men, and it becomes increasingly more common with age [2].

By analyzing the 5-year survival rate for early stage it reaches 60–95%, while it drops dramatically to 35 % with lymph nodes involvement, indicating that early disease detection and treatment are necessary to improve the management of CRC patients [3]. It is estimated that about 15-30 % cases of CRC have a major hereditary component [4, 5], however more than 70 % of colorectal cancers develop from sporadic adenomatous polyps [Figure 1], [6].

Even if this disease is curable in early stages, frequently the tumor becomes metastatic by the time an individual presents to their physician with symptoms and thus, the mortality is very high. Therefore, increasing efforts are being focused on developing more effective screening and prevention measures for colorectal cancer [7].

Contributory agents and mechanisms in CRC include dietary and lifestyle factors and inherited and somatic mutations. Among the most significant dietary and lifestyle risk factors for CRC, exogenous factors, such as consumption of red meat and alcohol, smoking and obesity has been suggested as possible risk factors, while an hypocaloric diet, high in dietary fiber and low in fat seem to be protective, especially if combined with physical activity [6]. Moreover estrogen, calcium, nonsteroidal anti-inflammatory drugs and some statins protect against CRC [8, 9].

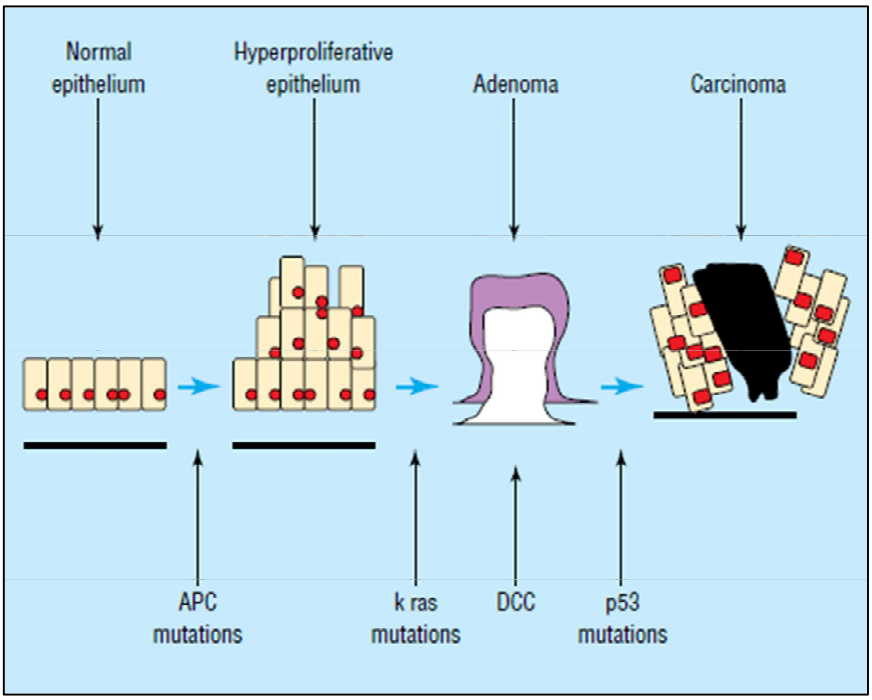

Figure 1: Proposed adenoma to carcinoma sequence in colorectal cancer. Reproduced from Parkin DM., Pisani P., Ferlay J. Global cancer statistics. CA Cancer J Clin. 1999; 49(1):33-64, 1.

All of these factors have led to the theory that CRC is a heterogeneous multifactorial disease [10]. According to this theory, CRC comes out across multiple and sequential steps where genetic and epigenetic alterations are accumulated. It is of note that not only the combination, but also the timing of the molecular alterations is critical for neoplastic pathway determination [11].

The prognosis of CRC is affected by the mutational status of several genes. Tumorigenesis and tumor progression in CRC result from multiple genetic and epigenetic abnormalities, including defective DNA mismatch repair and mutation of KRAS, NRAS, BRAF, PI3K, PIK3CA and p53 [12, 13, 14]. These (epi)genetic changes may affect the survival of CRC patients.

A large body of evidence suggests that there are three different pathogenetic pathways involved in both sporadic and hereditary tumor development: chromosomal instability (CIN), microsatellite instability (MSI) and CpG island methylator phenotype (CIMP); while the involved epigenetic events are modifications in histone proteins, DNA methylation, and miRNA aberrations [10, 15].

CIN refers to an accelerated rate of gains and losses of portions of chromosomes. CIN is characterized by accumulation of mutation in tumor suppressor genes and oncogenes, such as APC and KRAS, and loss of heterozygosity (LOH) [12].

MSI, elongation or shortening of the microsatellite, is primarily due to inactivation of DNA mismatch repair (MMR) genes, which are responsible for correcting base-base DNA replication errors. Typical for MSI tumors are frameshift mutations in specific genes such as β-catenin, transforming growth factor β receptor II (TGFβRII), epidermal growth factor receptor (EGFR) or Bcl-2-associated X protein (BAX) [16, 17].

Aberrant hypermethylation in CpG-rich promoters is a common feature of human neoplasia, associated with transcriptional inactivation of tumor suppressor genes or other tumor-related genes [13]. In the colorectum, DNA hypermethylation in CpG-rich promoters defines a distinct tumor subgroup [18], associated with proximal colon localization, older age, MSI, high frequency of BRAF and KRAS mutations and poor differentiation [14].

Tumor heterogeneity

It has been known for a long time that tumors are characterized by extensive intratumoral heterogeneity, indeed cells within a tumor exhibit tremendous variability due to the degree of molecular and phenotypic heterogeneity, making it difficult to develop therapies, particularly for more advanced metastatic disease. The dynamic variability of cell populations provides the driving force for tumors in order to evolve and enhance the robustness of tumors [19].

Differences exist not only within a single tumor, but extensive variations exist also among tumors of individual patients presenting with cancers arising from the same tissues, and between primary and metastatic tumors (intertumor heterogeneity) [19, 20]. Thanks to increasing knowledge of intertumor heterogeneity, it was possible to obtain a large classification of tumor subsets according to the differentiation grade, staging, cellular morphology and marker expression [20].

Since not only mutations offer selective growth advantage, just mutations that deeply contribute to tumor initiation and progression (driver mutations) could help to determine appropriate therapeutic targets [21]. It is increasingly being recognized that the classification of colon cancer patients has to be based on whole –genome expression data, rather than focusing in a single mutation [22, 23] in order to better select patients for targeted therapy. According to that, Cortes J. et al [24] suggest to manage similarly cancers from different organs that share common molecular mutations.

A large body of evidence suggests that, although tumor heterogeneity is primarily the result of genetic instability, the dynamic variability of cell population is driven also by epigenetic changes [20, 25], key factors for the formation of the most tumor initiating cell subpopulations in cancer [Figure 2].

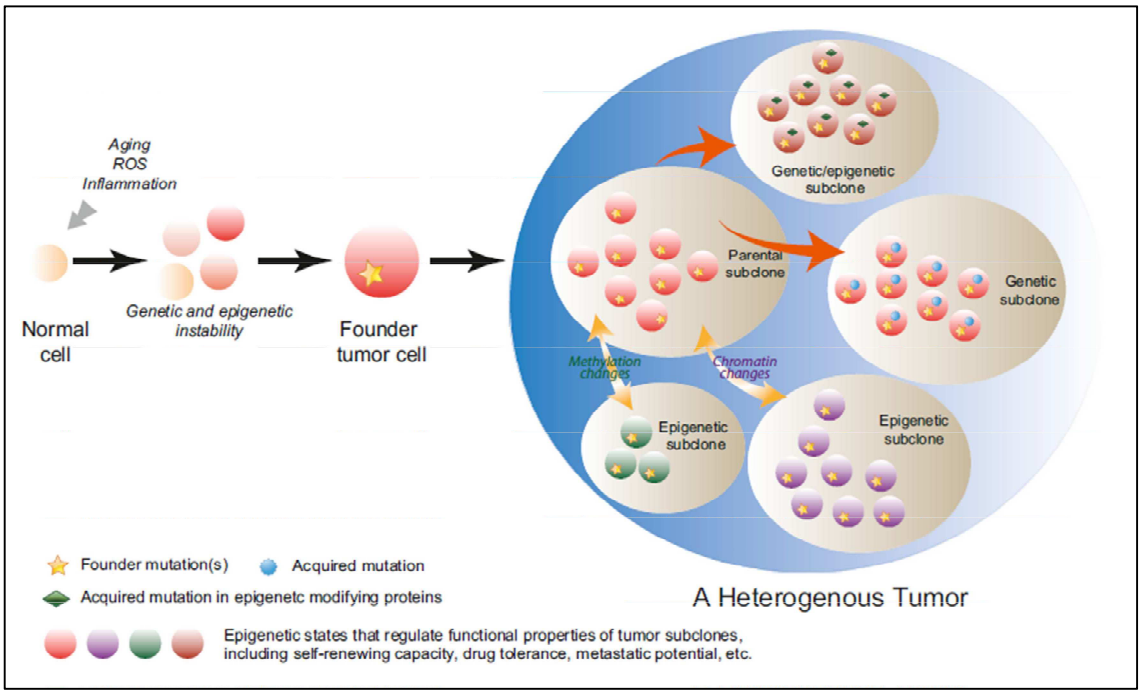

Figure 2: Genetic and epigenetic contributions to tumor heterogeneity. During oncogenesis, environmental stress may promote clonal expansion of cells with genetic or epigenetic abnormalities. These cells then acquire further mutations or epigenetic alterations and become founder tumor cells that initiate precancer or cancer. In an established tumor, the parental subclone may acquire new driver or passenger mutations (genetic subclone), or undergo epigenetic alterations on the levels of chromatin or DNA methylation, or both (epigenetic subclones). Some subclones may acquire mutations in epigenetic modifying proteins resulting in emergence of epigenetic changes (genetic/epigenetic subclones). Reproduced from Easwaran H., Tsai HC., Baylin SB. Cancer Epigenetics: Tumor Heterogeneity, Plasticity of Stem-like States, and Drug Resistance. Mol Cell. 2014; 54(5):716-27.

Tumor heterogeneity is also influenced by the cell of origin and involves the coevolution of tumor cells with nonmalignant stromal cells, that establish a tumor microenvironment by mediating changes in clonal evolution rate or stem cell content [25, 26], [Figure 3]. In the context of "tumor stem cell" population, Greaves et.al [27], proposed a model for the evolution of cancer in which the initial oncogenic mutations result in transforming progenitor cell, that, acquired the aberrant properties to growth, became substrate for tumor progression.

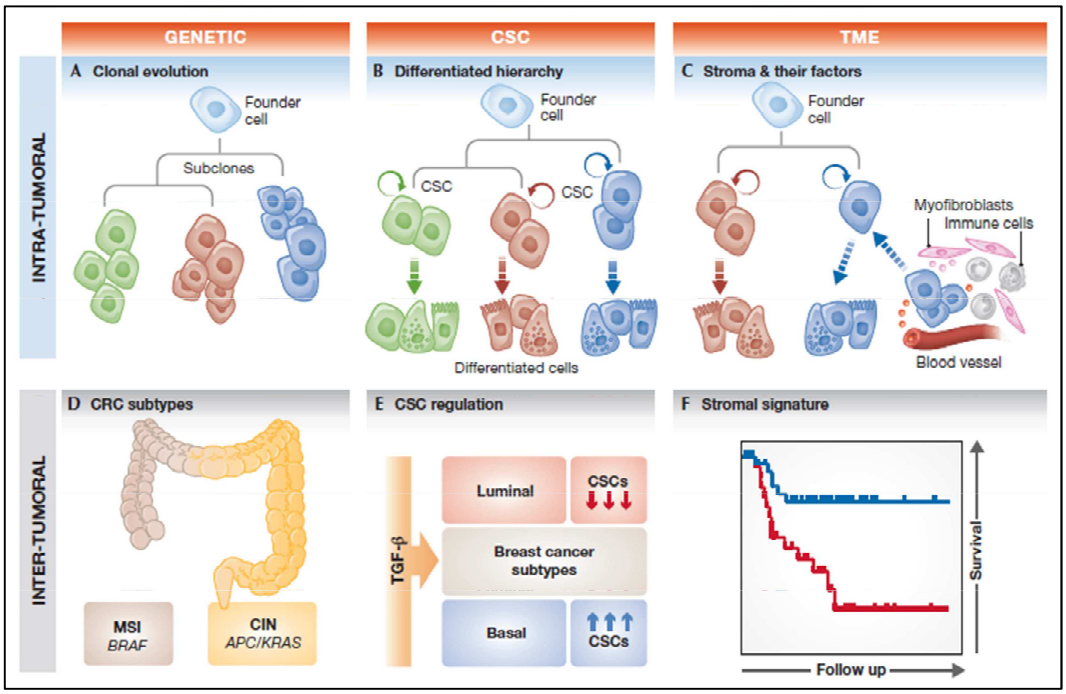

Figure 3: Cartoon representation of several factors affecting tumor heterogeneity. Reproduced from De Sousa E Melo F., Vermeulen L., Fessler E., Medema JP. Cancer heterogeneity—a multifaceted view. EMBO Rep. 2013; 14 (8):686-95.

As tumors progress, multiple environmental pressures may promote clonal expansion of cells with genetic and epigenetics abnormalities in order to select the best endowed clones to respond to these changes. In their paper Fearon et. al [26], indicate that the amount of mutations is correlated with more advanced disease and, significantly, they suggest a preferential sequence of mutation events at each stage.

According to the role of epigenetic to tumor heterogeneity certain subtypes of CRCs and gliomas have been defined by a high level of methylation at the CpG rich promoter regions of a subsets of genes [28, 29].

From a therapy point of view genetic and epigenetic heterogeneity translates into different diagnostic signatures that will have implications for therapeutic approaches [Figure 4]. Most

targeted mutations occur in the founder clone [Figure 4A], and when treated with targeted therapies, a pre-existing drug- tolerant clone could remain unaffected.

Similarly epigenetic alteration can develop from targeted chemotherapy [Figure 4B], however the drug tolerance could be reversed and cells return to the sensitive epigenetic state after prolongated treatment with epigenetic therapy, such as low-dose histone deacetylase (HDAC) inhibitors or DNA demethylating agents. Finally it is known that epigenetic therapy could convert cancer cells in a drug-resistence state that was not active for the original cancer population [Figure 4C], [25].

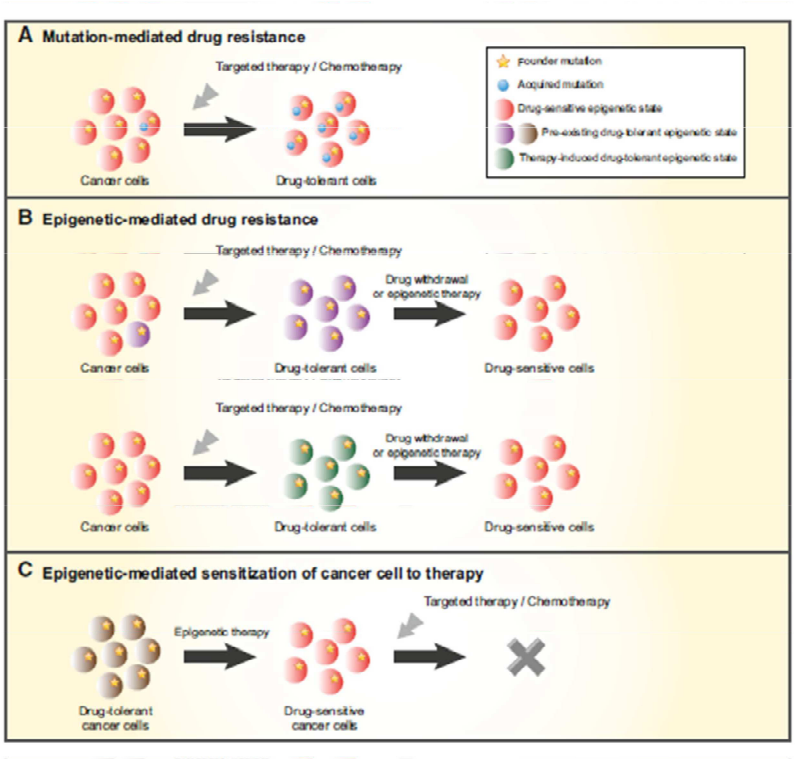

Figure 4: Genetic and epigenetic mechanisms for drug resistence and implications of epigenetic therapy: contributions to Tumor heterogeneity. Reproduced from Easwaran H., Tsai HC., Baylin SB. Cancer Epigenetics: Tumor Heterogeneity, Plasticity of Stem-like States, and Drug Resistance. Mol Cell. 2014; 54(5):716-27. 5, 2014.

The role of the tumor microenvironment

Mounting evidence from various experimental systems has demonstrated a role of tumor microenvironment in tumor initiation and progression. Since the tumor microenvironment (TME) was lately recognized as the product of a developing crosstalk between different cells types, it plays an important role as well in determining the heterogeneity observed within and across tumors. Physiologically, the stromal environment contains many distinct cell types, consists of a dynamic framework of extracellular matrix components (collagen, fibronectin, proteoglycans etc) intermingled with endothelial cells and their precursors, pericytes, smooth muscle cells, fibroblasts, carcinoma-associated fibroblasts, myofibroblasts, neutrophils, eosinophils, basophils, mast cells, T and B lymphocytes, natural killer cells and antigen presenting cells (APC) such as macrophages and dendritic cells [30, 31]. The only presence of TME components is, by itself, a source of heterogeneity, and this cell types can be distributed in different tumor microenvironments, such as the invasive or noninvasive compartment. The successful expansion of malignant tumors requires an active collaboration between malignant and stromal cells via heterotypic cellular interactions [30], [Figure 5].

The driving forces of tumour microenvironmental evolution are genetic instability of malignant cells and environmental selection forces, which include endogenous, tumour-growth-induced stress stimuli, such as hypoxia, acidosis, starvation, oxidative stress, biomechanical stress and immunoediting as well as exogenous stresses, for example, therapeutic interventions. Extrinsic factors produced by stromal cells can influence the tumor heterogeneity changing stem cell content; for instance chronic inflammation can drive to oxidative stress and contribute to the increase of DNA damage. In this way it is possible to increment the intra-tumor heterogeneity localizing inflammation in particular tumor regions, as well condition cancer subtypes that are associated strongly with chronic inflammation [20].

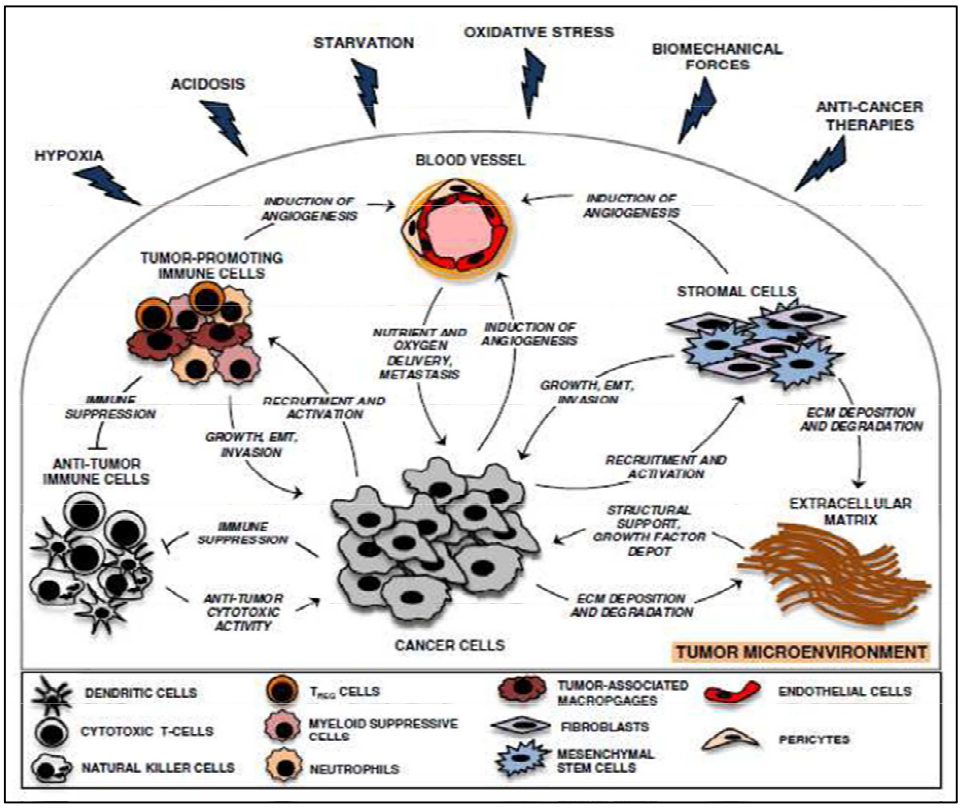

Figure 5: Heterotypic cellular interactions in the tumor microenvironment. Reproduced from Kucharzewska P., Belting M. Emerging roles of extracellular vesicles in the adaptive response of tumour cells to microenvironmental stress. J Extracell Vesicles, 2013.

For instance, tumor-associated myofibroblasts produce HGF that binds to c-MET and activates Wnt activity to support colon CSCs [31]; more recently Lu J et al. have shown a similar effects about Jagged1 [32]. Altogether, these studies have shed light on the impact of the TME on tumor heterogeneity. The role of factors provided by tumor-associated cells is not only in keeping cell attributes, but also in inducing the phenotype in more differentiated cells. For instance, HGF is able to induce differentiation of colon cancer cells to revert to a CSC state [31], and in the same way TGF-β triggers an EMT–CSC programme in mammary epithelial cells [33].

Cancer cells and stromal cells communicate by direct cell-to-cell contacts as well as the release of signalling molecules, such as soluble growth factors and chemokines that induce an altered ECM providing additional oncogenic signals that enhance cancer-cell proliferation and invasion [33]. A new class of cancer therapies that targets this pathological communication interface between tumor cells and host cells is currently under development.

An important component of the tumor microenvironment is the tumor vasculature. The formation of a tumor-associated (angiogenic) vasculature is essential for tumor progression. The development of the tumor vasculature is regarded to derive from both the pre-existing vessels via endothelial cell migration and proliferation (angiogenesis) and recruitment of progenitor cells from bone marrow (vasculogenesis). Tumor-associated vessels promote tumor growth by providing oxygen and nutrients and favor tumor metastasis by facilitating tumor cell entry into the circulation [29]. Tumor angiogenesis is initiated during tumor progression (‘angiogenic switch’) that often occurs at the time of the conversion from premalignant to malignant lesions. Tumor angiogenesis is determined by the balance between the genetic status of the tumor itself, signals from stromal, recruited inflammatory cells and by the appearance of hypoxia circulation [29]. Several studies have shown that the dynamic crosstalk between endothelial cells and other stromal cells substantially contribute to tumor angiogenesis.

Tumor progression and metastasis formation

Metastases represent the end products of a complex series of cell-biological events, which are collectively termed the invasion and metastasis cascade. During metastatic progression, tumor cells need to detach from the primary tumor growth and intravasate into blood vessels to enter the circulation. Once in the circulation, cells can be traslocated sistemically over long distances towards other organs. Some cells remain dormant for a long time before they start the formation of metastatic foci. It is known that the interaction with the non neoplastic stromal cells contributes to the behavior of tumor cells in these distant organs [34], [Figure 6].

Although the distribution of metastases may depend on the mechanical force of blood flow, it has been recognized that metastasis is a non-random process, since it is clear that certain types of cancer preferentially metastasize to particular sites, while other types favor other remote organs for metastasis formation. This organ selectively was described in 1889 by Steven Paget, who proposed “the seed and soil” hypothesis based on his observations. He postulated that the successful colonization of a secondary organ depends on the intrinsic properties of the tumor cell itself (seed) and on a permissive and supportive environment (soil), which co-operate to allow for the survival and proliferation of the cancer cells [35].

The first step in tumor progression is most likely favored by the heterogeneity of cells forming a primary tumor. The intrinsic genomic instability of tumor cells causes an increase in mutation frequency necessary to acquire metastatic capacity. DNA integrity can be prejudiced by aberrant cell-cycle progression, alteration in epigenetic control mechanisms or inactivation of DNA repair genes. For instance 50 % of cancers have a loss-of-function mutation in the tumor suppressor protein p53 [36] that allows the accumulation of cells with DNA damage.

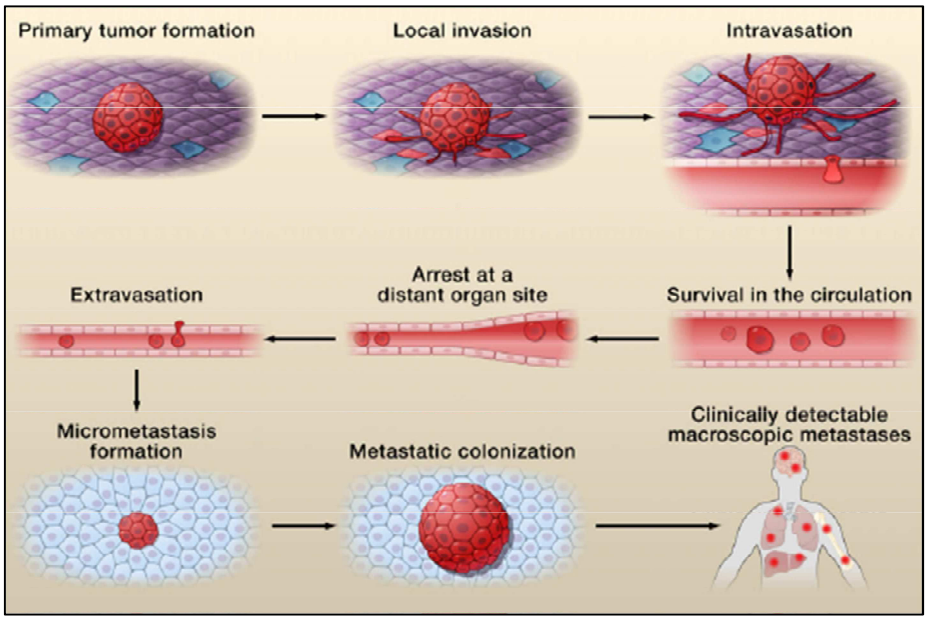

Figure 6: The invasion metastasis cascade. Reproduced from Valastyan S., Weinberg RA. Tumor Metastasis: Molecular Insights and Evolving Paradigms. Cell. 2011; 147(2):275-92.

In order to invade the stroma, carcinoma cells have to break the basement membrane (BM) that represents an intrinsic barrier to invasiveness. At a cell-biological level, most kinds of carcinoma are able to invade in a cohesive manner through a process called "collective invasion". Moreover, individual cancer cells can overrun the BM by two different programs: the protease-, stress-fiber and integrin-dependent "mesenchymal invasion" mechanism or the protease-stress- fiber and integrin-indipendent Rho/Rock-dependent "amoeboid invasion" program [37]. Supposedly cancer cells could interconvert between these two different kinds of invasion in response to microenvironment stimuli.

Loss of the BM barrier lets direct invasion of the carcinoma cells of the stromal compartments where tumor cells become exposed to environmental stresses, including a low pH, reactive oxygen species, mediators of the inflammatory response, and a lack of oxygen caused by an increased distance from blood vessels providing oxygen and nutrients [38] [Figure 7]. These stromal cells are able to influence the aggressive behavior of cancer cells by different types of

heterotypic signals. For instance, cellular hypoxia causes activation of the transcription factor Hypoxia Inducible Factor (HIF) that induces gene expression that leads to changes in anaerobic metabolism, angiogenesis, invasion, and survival [39]. Staller et al. [40] showed that a product of HIF-induced gene activation, the chemokine receptor CXCR4, together with its ligand, the chemokine stromal-cell-derived factor1 (SFD-1), allow the survival of cancer cells at sites of metastasis in breast cancer and renal-cell cancer. By HIF-dependent transcriptional activation of the gene encoding vascular endothelial growth factor (VEGF) new blood vessels are formed in the expanding tumor mass to restore the levels of oxygen [39]. All together these signals, produced by microenvironment and tumors cells, provide abundant opportunities for cancer cells to directly invade the systemic circulation entering into the lumina of lymphatic or blood vessels.

A large body of evidence suggests that different molecular changes can help tumor cells to cross the pericyte and endothelial barrier of microvessels. For instance Sonoshita et al. show a role of the transcriptional modulator amino-terminal enhancer of split (Aes) in the inhibition of the intravasation of colon cancer cells injuring trans endothelial barrier by Notch signaling [41]. Additionally, the cyclooxygenase-2, epiregulin (EREG), MMP-1, and MMP-2 in a synergistic manner stimulate neoangiogenesis [38].

In distant organ sites, circulating tumor cells have to survive a variety of stress and evade immune response. In this context Joyce et al. [42] have shown that tumor circulating cells form microemboli through interaction with L- and P-selectins in order to bypass immune detection and better persist within the circulation until they arrest at distant organ sites. Demicheli et al. [43], suggest that, in breast cancer patients, metastatic foci after surgery of the primary tumor do not show continuous growth over time, but show a form of a quiescent stem cell-like state. This stem cell-like state, with a low proliferation capacity, might make

tumor cells invisible for the immune system and anti-cancer drugs which target highly proliferating cells.

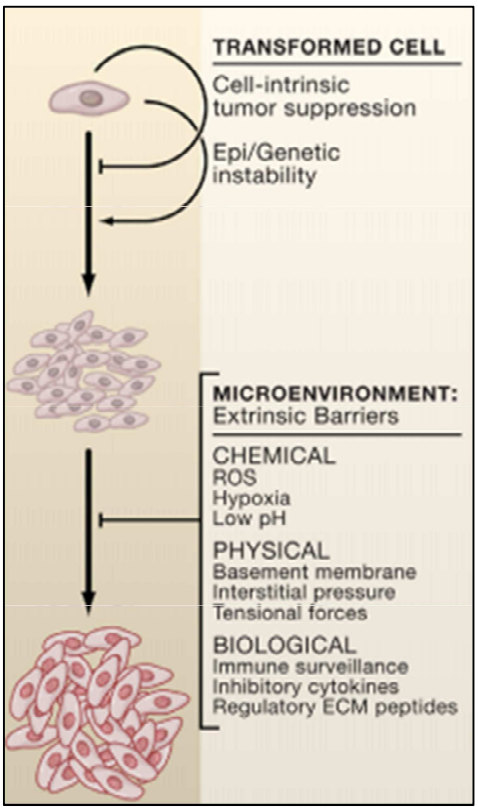

Figure 7: Pressures that drive selection for metastatic traits. Reproduced from Gupta GP., Massagué J. Cancer. Metastasis: Building a Framework. Cell. 2006; 127(4):679-95.

Exosomes: biogenesis, composition, release and uptake of exosomes by target cells

Cell to cell communication is an essential process that coordinates the activities among different kinds of cells. Historically cells are thought to communicate with each other by direct contact (juxtacrine signaling) or by soluble mediators (autocrine, paracrine, and endocrine signaling). Moreover, over the last few years, an increasing amount of studies have shown that cells are able to exchange information through a sophisticated method based on the release of specialized membrane-enclosed particles called extracellular vesicles (EVs) [44, 45]. Current criteria to distinguish among different EV populations are based on size, density, subcellular origin, function and molecular cargo. The EVs can be divided into three main classes: exosomes, microvescicles (MVs) and apoptotic bodies. While exosomes are biological nanovescicles (40-100 nm) that are formed by the endocytic pathway, apoptotic bodies (50–500 nm) are released by cells undergoing programmed cell death, and microvescicles, are derived directly from the plasma membrane (100– 1000 nm for microvescicles) [Figure 8], [46].

EVs have been originally also named on the basis of their tissue origin; for example, prostasomes are vesicles secreted by prostate epithelial cells and secreted into the seminal fluid, while oncosomes, vescicles released by cancer cells [47].

Many different cell types, are able to secrete exosomes and MVs, under both normal and pathological conditions, including red blood cells, dendritic cells, fibroblasts, epithelial and tumor cells [44].

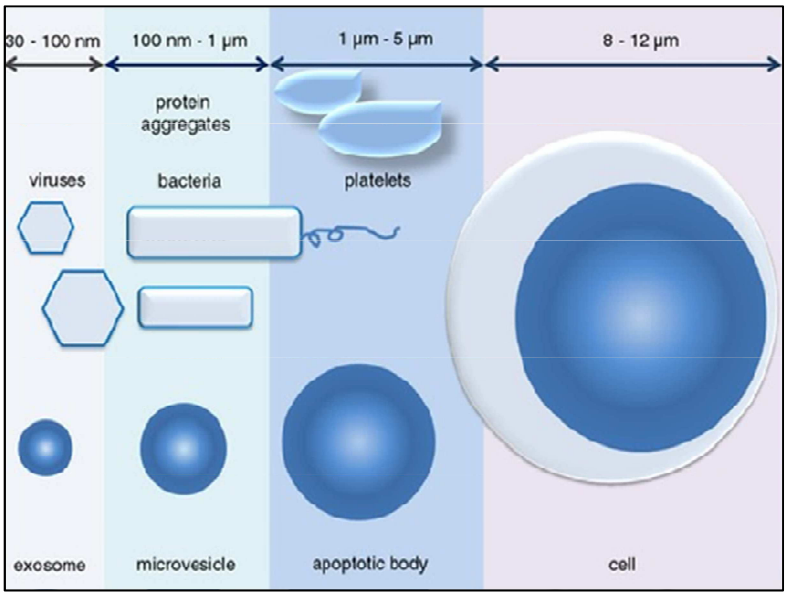

Figure 8: Sizes of different types of membrane vesicles. Reproduced from György B et. al. Membrane vesicles, current state emerging role of extracellular vesicles. Cell Mol Life Sci. 2011; 68(16):2667-88.

Among EVs, exosomes have recently received most of the attention. Initially exosomes were described as vesicles released by reticulocytes in order to remove unnecessary proteins, such as the transferrin receptor, during the maturation process into erythrocytes [45]. However there are emerging evidence that indicates exosomes as important players, within a tissue microenvironment, in cell to cell communication.

The first step in exosomes biogenesis [48] is the formation from the intraluminal vesicles (ILVs) of multivesicular bodies (MVBs) as a part of endocytic pathway known as late endosomes. MVBs can either fuse with lysosomes for degradation or travel back to and fuse with the plasma membrane [44, 45, 47]. This process encapsulates cytoplasmic RNA molecules and functional proteins into exosomes [Figure 9]. The mechanisms of assembly and sorting of exosomes are not well defined, but several molecules have been shown to regulate this process, such as RAB11, RAB27, RAB35, and syndecan-syntenin-ALIX. Moreover the ESCRT (endosomal sorting complex required for transport) member TSG101

(tumor susceptibility gene 101) and the tetraspanin CD63, which is enriched in specific plasma membrane domains involved in microvesicles budding, have both been described as involved in exosome formation.

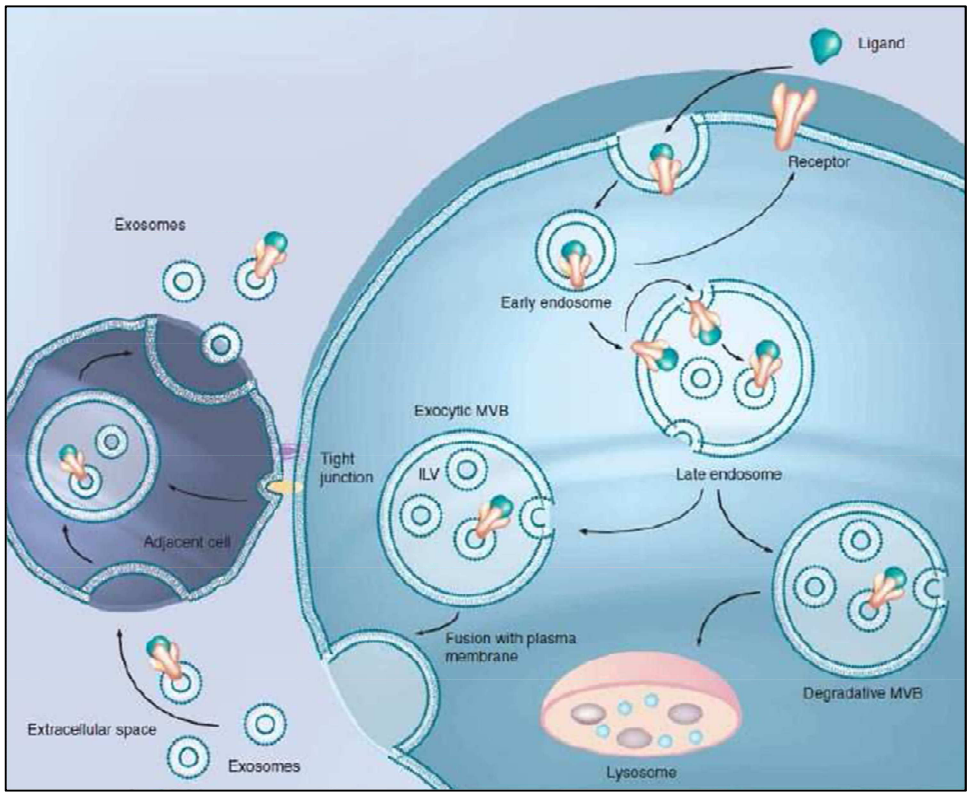

Fig. 9: Exosome generation. A receptor is internalized following ligand binding and is trafficked to early endosomes. In early endosomes, proteins are either recycled to the plasma membrane or sequested in ILVs of the MVBs. MVBs can be either degradative (evolving into lysosomes) or it can be exocytic (fuse with plasma membrane to release its contents). The exocytic MVBs fuse with the plasma membrane to release exosomes to the microenvironment. Released exosomes can be internalized by neighboring cells and mediate some functions. Reproduced from Simpson RJ., Lim JW., Moritz RL., Mathivanan S. Exosomes: proteomic insights and diagnostic potential. Expert Rev Proteomics. 2009; 6(3):267-83.

However, recently, the consideration of the tetraspanin CD63 as a specific exosomal marker has been reevaluated, since this protein has also been found in other EV subtypes [49].

Due to their endosomal origin, all exosomes contain membrane transport and fusion proteins (GTPases, Annexins, flotillin), tetraspannins (CD9, CD63, CD81, CD82), heat shock proteins (Hsc70, Hsp 90), proteins involved in multivesicular body biogenesis (Alix, TSG101), as well as lipid-releated proteins and phospolipases [50], [Figure 10].

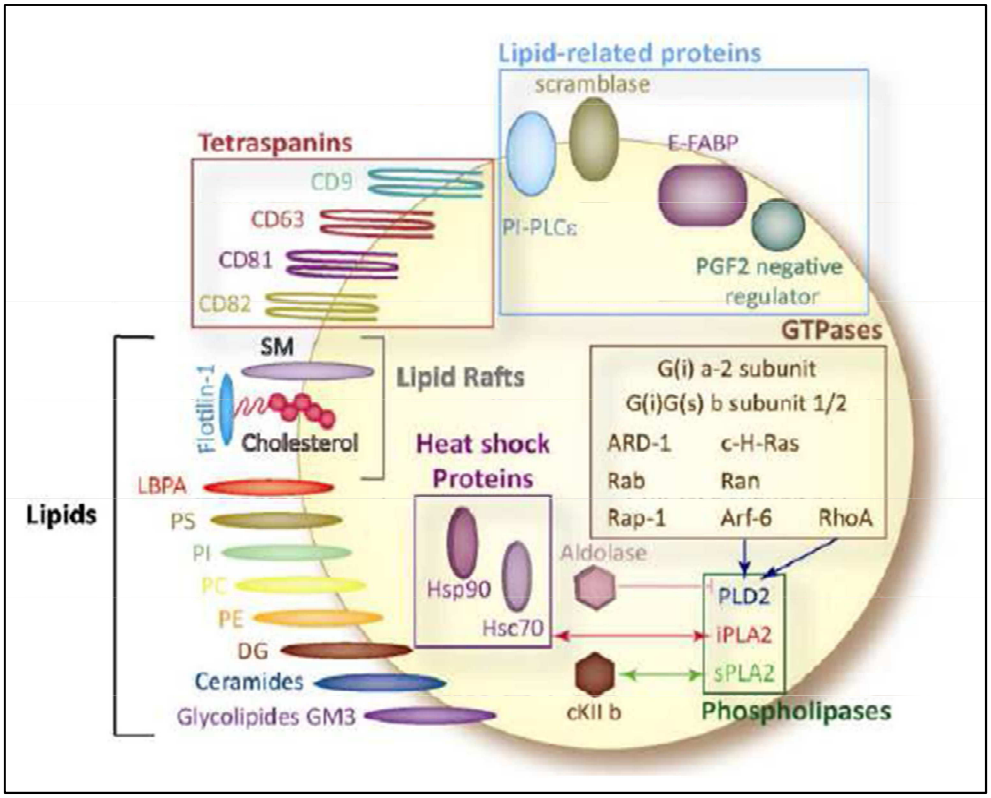

Figure. 10: Common molecular components of exosomes. Reproduced from Record M., Subra C., Silvente-Poirot S., Poirot M. Exosomes as intercellular signalosomes and pharmacological effectors. Biochem Pharmacol. 2011; 81(10):1171-82.

Although exosomes from different sources have a common set of proteins representing molecules that regulate membrane cytoskeleton dynamics and membrane fusion events, exosomes also contain some specific proteins reflective of the parental cell. For instance epithelial tumor cells secrete exosomes carrying the epithelial cell adhesion molecule (EpCAM) [51], melanoma-derived exosomes contain the tumor-associated antigen Mart [52];

while perforin and granzyme are found on cytoxic T-lymphocytes [53], and subunits of glutamate receptors on neurons [54].

Exosomes secretion can be constitutive or inducible depending on the cell type. Levine's group demonstrated that mouse embryo fibroblasts with a wild-type p53 gene produced exosomes after DNA damage but isogenic MEFs with no p53 genes (from knockout mice) failed to produce exosomes after the dame genotoxic stress. A p53-regulated gene product, TSAP6, was shown to be involved in exosomes production thus alerting adjacent cells and the immune system of these events. [55].

The mechanism associated with exosomes internalization occurs in a non-random process, but it is still poorly understood. Recent studies indicate that the tetraspanin-integrin complex contributes considerably in targeting enabling the binding of exosomes to target cells [56, 57]. Moreover, a pro- inflammatory environment may enhance the expression of receptor molecules such as ICAM-1 on the membrane surface, which increases the exosomes adhesion to the target cells [58].

Both fusion and active endocytosis have been proposed as mechanisms for exosomes uptake [59-61].

As shown in Figure 11A [45], exosomal membrane proteins can interact with the target cell in a juxtacrine fashion, acting as ligands for receptors on the cell surface. Additionally, exosomes can also fuse with the target cell resulting in the nonselective transfer of proteins and RNA from the exosome to the target cell [Figure 11B]. Finally, in a recent paper Feng et al. showed that in phagocytic cells, exosomes can be internalized efficiently via phagocytosis in an actin-cytoskeleton and phosphatidylinositol 3-kinase –dependent manner [Figure 11C], [59]. Their experimental data demonstrated that exosomes adhered easily to the cell surface of non phagocytic cells but could not be internalized, as they could be removed by trypsinization

or with extensive acid washing. In contrast, the same treatment did not remove exosomes from phagocytes, as they were already inside the cell. Finally, once inside the recipient cell, exosomes can release their content through fusion with endosome membrane or can be targeted to lysosomes for degradation [44].

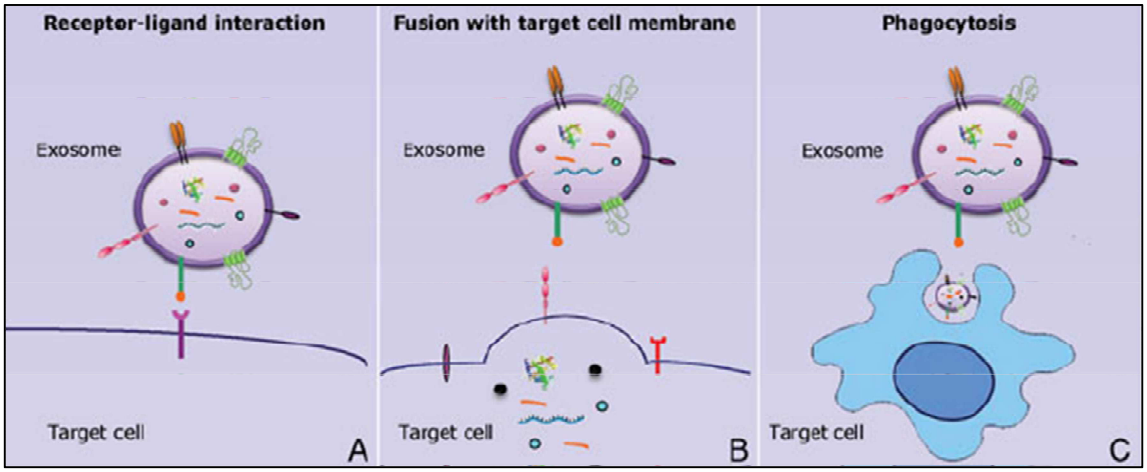

Figure 11: Mechanisms of intercellular communication mediated by exosomes. (A) Exosomes can bind to cells through receptor-ligand interactions and activate intracellular signaling. (B) Exosomes can fuse with the target cell membrane and deliver exosomal membrane and cytoplasm proteins to the recipient cell. The plasma membrane of the target cells can be also modified by the addition of new membrane receptors and different lipid components. Exosomal molecules (proteins, mRNAs, and miRNAs) can activate a multitude of signaling events in the recipient target cell. (C) An alternative exosome–cell interaction mechanism is represented by phagocytosis. Reproduced from Fontana S., Saieva L., Taverna S. and Alessandro R. Contribution of proteomics to understanding the role of tumor-derived exosomes in cancer progression: State of the art and new perspectives. Proteomics. 2013; 13(10-11):1581-94.

Functional relevance of exosomes in cancer progression

Cancer cells begin to modulate their stromal environment starting at early phases of the neoplastic process mainly by pathways involving cell-to-cell contact and the release of soluble factors, such as TNFα, TGFβ, VEGF, that are able to influence the recruitment of different cell type. Recently, exosomes have been considered as new vehicles that exchange proteins and genetic materials into the tumor microenvironment. Tumor derived exosomes (TDEs), seem to have dual functions: they can manipulate the local and systemic environment to aid cancer growth and dissemination, as well TDEs may also program the immune system to elicit an anti-tumor response.

These effects [Figure 12] are essentially due to the ability of TDEs to contribute to the establishment of a premetastatic niche by promoting angiogenesis, extracellular matrix (ECM) degradation, and stromal remodeling. TDEs can interfere with the action of therapeutic agents by inducing drug resistance. TDEs are also involved in transferring microRNAs (miRNAs) and mRNAs to neighboring cells, thereby inducing gene expression modulation [45].

Several studies have reported that TDEs may function in an autocrine or paracrine manner. Luga and collaborators have recently shown that cancer associated fibroblast (CAF) secrete exosomes that are able to promote, in an autocrine manner, breast cancer cell protrusive activity and motility by WNT-planar-cell polarity (PCP) signaling [62]; in this regard TDEs recruitment of fibroblasts could support tumor angiogenesis.

Several studies have revealed the role of TDEs in activating signal transduction pathways involved in cancer cell proliferation and survival. Tumor-derived exosomes may also transport apoptosis inhibitory proteins, induced under stress conditions, to promote tumor survival.

One of the first evidence supporting this role was proposed by Rak and collaborators which demonstrated that the intercellular transfer of the oncogenic receptor EGFRvIII, mediated by TDEs to glioma cells lead an augmented expression of anti-apoptotic genes and an increase in anchorage independent growth capacity [63]. Survivin, a member of the inhibitor of apoptosis protein family, can be absorbed by cancer cells from extracellular media and inhibit their apoptosis following genotoxic stress as well as increase their replicative and metastatic ability [64]. Colon cancer cells harboring only mutant KRAS alleles are capable of releasing exosomes with mutant KRAS proteins [65], leading to a growth advantage in the recipient non-transformed wild-type KRAS-expressing cells.

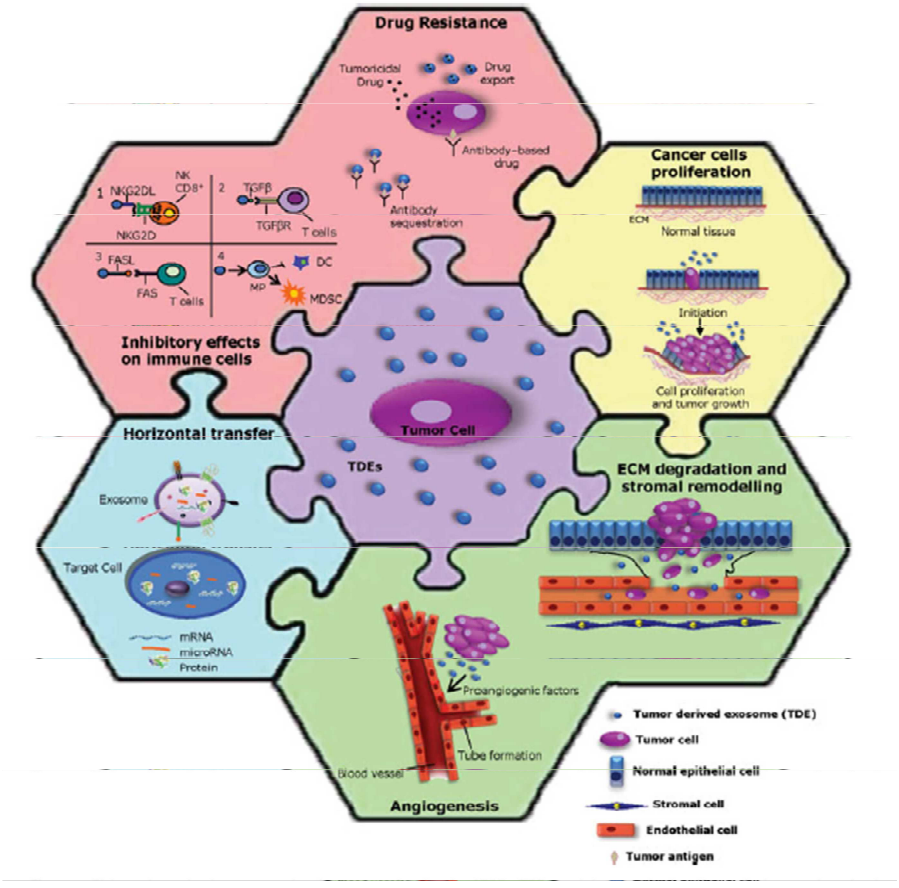

Figure 12: Pleiotropic mechanisms supporting the protumorigenic role of TDEs. Reproduced from Fontana S., Saieva L., Taverna S. and Alessandro R. Contribution of proteomics to understanding the role of tumor-derived exosomes in cancer progression: State of the art and new perspectives. Proteomics. 2013; 13(10-11):1581-94.

Another mechanism that seems to play a role in cell-cell communication within the tumor microenvironment is the intercellular exchange of proteins and genetic materials via exosomes [66]. In particular, transport of mRNAs and microRNAs, from tumor cells to neighboring cells could have significant effects on tumorigenesis. It has been suggested that the ability of exosomes to deliver nucleic acids to distal cells also makes them ideal candidates for gene therapy [67].

Additionally preliminary results suggest that exosomes mediate the transfer of mRNAs, miRNAs, and/or proteins, involved in drug resistance that drive the phenotypic changes of recipient cells. Exosomes may carry proteins involved in multidrug resistance or alternatively sequester the chemotherapeutic agent thereby decreasing the intracellular amount. For instance, exosomes from two docetaxel resistant prostate cancer cell lines can confer chemoresistance to non-resistant prostate cancer cell lines via exosomes mediated transfer of drug transporter, MDR-1 [68].

In addition to enhancing the invasiveness of cancer cells, TDEs contribute to the establishment of a metastatic niche via delivery of proteins, mRNAs and miRNAs that support angiogenesis. Jung et al. show for the first time how cancer-associated exosomes participate in the formation of the pre-metastatic niche in a rodent pancreatic cancer model [69]. Similarly, another study has shown that melanoma-derived exosomes enhance the lung endothelial permeability and increase lung metastases in mice [70]. In the same study, Peinado et al. demonstrated that melanoma cell derived exosomes are capable of recruiting bone-marrow derived cells to initiate a premetastatic niche, through the activation of the MET receptor tyrosine kinase.

Collectively, these studies indicate that tumor-derived exosomes play a crucial role in manipulating the tumor microenvironment for the benefit of cancer cells.

Aims

A large body of evidences suggests that tumors are characterized by extensive intratumoral heterogeneity that provides the driving force for tumors in order to evolve and enhance the robustness of cancer. From a therapeutic point of view the dynamic variability of cell populations makes difficult to develop new treatments, particularly for more advanced metastatic disease.

Since the tumor microenvironment was lately recognized as the product of a developing crosstalk among different cells types, it plays an important role as well as in determining the heterogeneity observed within and across tumors. Recently, a number of studies have described exosomes as new players in modulating tumor microenvironment, promoting angiogenesis and tumor progression. A better understanding of the molecular mechanisms and of molecules that drive such processes could lead to the identification of new targets.

On the bases of the data shown in literature the overall aims of this project is to understand, in the context of the tumor heterogeneity and by using isogenic cell lines derived from colorectal cancer, if exosomes could be, not only simply vehicles, but new actors between more and less aggressive cancer cells and if they are able to induce phenotypic changes in neighboring cells by activating specific cell signaling pathways, leading to cancer progression.

More specifically, the aims of this thesis are to:

- ✓ Test if the addition of exosomes derived from colon cancer metastatic cell line (SW620) is able to induce a more aggressive phenotype in colon cancer non metastatic cell line (SW480).

- ✓ Evaluate if exosomes derived from cell line with different metastatic potential may differently affect the behavior of endothelial cells, that are important components of the tumor microenvironment.
- ✓ Understand the molecular mechanisms by which exosomes derived from metastatic cell line are able to influence the behavior of the different cells belonging to the tumor microenvironment.

Materials and Methods

Cell culture

SW480 and SW620 cells (ATTC), were cultured in RPMI 1640 (Euroclone UK) supplemented with 10% FBS (Euroclone UK), 2mM L-glutamine (Euroclone UK), 100 U/ml penicillin and 100 mg/ml streptomycin. Human umbilical vein endothelial cells (HUVEC, Lonza, Clonetics, Verviers, Belgium) were grown in endothelial growth medium (EGM) supplemented with Hydrocortisone, hFGF-B; VEGF; R3-IGF-1; Ascorbic Acid; Heparin; FBS; hEGF; GA-1000; EGM®-2 BulletKit® (Clonetics CC-3162). SW480 and SW620 cells were maintained at 80 % of confluence to recover exosomes and/or large large extracellular vesicles. HUVEC cells were cultured in Petri dish, were harvested using trypsin-PBS 1:1 and seeded for the experiment. Cultures were grown placed in a humidified 95% air and 5% CO2 atmosphere at 37° C.

Isolation of exosomes and large extracellular vesicles

Exosomes and large extracellular vesicles produced by SW480 and SW620 cells during a 24 hr culture period, were isolated from conditioned culture medium supplemented with 10% FBS (previously ultracentrifuged) by differential centrifugation. Conditioned medium (CM) was recovered after 24h. Briefly, cells and debris were eliminated by centrifugation at 300 g for 5 min. The supernatant was then centrifuged at 10,000 g for 30 min to precipitate large EVs. For isolation of nano-sized EVs, the supernatant remaining after the 10,000 g spin was

filtered (0,22µm filter) and subjected to additional centrifugation at 100,000 g for 1h and 45 in SW 28 rotor. Pellet was washed and then resuspended in PBS.

To further verify the identity of large extracellular vesicles and exosomes, two different standard protocols were carried out, the sucrose or iodixanol gradients.

The 30%sucrose/D2O cushion (density of 1.13–1.19 g/mL) was carried out as described by Lamparski et al [71]. Exosomes from differential centrifugation method were resuspended in 25 ml of PBS. 4ml of 30%sucrose/D2O was loaded on the bottom of the ultracentrifuge tube and diluted exosomes were layered above the sucrose cushion, gently without disturbing the interface. Samples were ultracentrifuged at 100000xg, 4°C for 75 min in SW 28 rotor. The cushion, which now contains exosomes, was recovered with a 5ml syringe from the side of the tube. The cushion was transferred to a fresh ultracentrifuge tube and were added 40 ml of PBS. Samples were ultracentrifuged at 100000xg 70 min in 70 Ti rotor. Pellet was resuspended in lysis buffer for western blots or in PBS for cell treatments.

For discontinuous centrifugation by iodixanol gradient we used a modified version of a previously applied protocol [72]. Briefly 60%, 50%, 40%, 30%, 25%, 15%, 10% and 5% solutions were made by diluting a stock solution of OptiPrep™ (60% aqueous iodixanol from Sigma) in 0.25 M Sucrose/0.9 M NaCl/ 120 mM HEPES, pH 7.4. The 10,000 x g and 100,000 x g pellets were mixed in the bottom layer and the following solutions carefully layered. Centrifugation was performed at 100,000 x g for 3h and 50 min at 4 °C with a SW28 Beckman rotor. Eight individual fractions were collected, washed with PBS, and after centrifugation at 100,000 x g for 1 h at 4 °C, the pellet from each fraction suspended in either PBS or lysis buffer.

Western blot

Colon cancer cells, exosomes and large oncosomes were lysed in lysis buffer (300 mM NaCl, 50 mM Tris HCl Ph 7.6, 0.1% Triton, 1 mM PMSF, 10 mg/ml leupeptin, 10 mg/ml aprotinin, 4 mM EDTA, 2 mM sodium orthovanadate, 10mMNaPPI, 100mMNaF) on ice for 1h. The lysates were clarified at high speed centrifugation for 20 min and an aliquot of the supernatant was assayed to determine protein concentration by the Bradford method. Cell lysates or EVs lysates (30µg per lane) were separated using 4-12% Novex Bis-Tris SDS-acrylamide gels (Invitrogen, Life Technologies, USA), transferred on Nitrocellulose membranes (Invitrogen, Life Technologies, USA), and immunoblotted with the following primary antibodies: HSC70, CD63, TSG101, Alix, Calnexin, CD81 (Santa Cruz), , CK18 (Abcam). All secondary antibodies were obtained from Santa Cruz Biotechnology (Santa Cruz Biotechnology, Inc., Santa Cruz, CA, USA). Chemiluminescence was detected using AmershamTM ECLTM Western Blotting Detection Reagents (GE Healhtcare, UK).

Dynamic Light Scattering (DLS) analysis

Exosome size distribution was determined by DLS experiments. Collected exosome samples were diluted 30 times to avoid inter-particle interaction and placed at 20°C in a thermostated cell compartment of a Brookhaven Instruments BI200-SM goniometer, equipped with a solid-state laser tuned at 532 nm. Scattered intensity autocorrelation functions g2(t) were measured by using a Brookhaven BI-9000 correlator and analyzed in order to determine the distribution P(D) of the diffusion coefficient D by using a constrained regularization method or alternatively a gamma distribution [73]. The size distribution, namely the distribution of hydrodynamic diameter Dh, was derived by using the Stokes-Einstein relation: D =

(kBT)/(3πη Dh), where D is the diffusion coefficient, kB is the Boltzman constant, η is the medium viscosity and T is the temperature. The mean hydrodynamic diameter of exosomes was calculated by fitting a Gaussian function to the measured size distribution.

Labeling and internalization of exosomes

SW480 and SW620 cell-derived exosomes were labeled with PKH26 (Sigma-Aldrich, Italy), according to the manufacturer's instructions. Briefly, exosomes collected after the 100,000×g ultracentrifugation, were incubated with PKH26 for 10 min at room temperature. Labeled exosomes were washed in PBS, centrifugated, resuspended in low serum medium and incubated with HUVEC cells or SW480 and SW620 cells for 3-6 hours at 37°C. After incubation, cells were processed as previously described [74]. Cells were stained with ActinGreenTM 488 Ready ProbesR Reagent (Life Technologies, USA) that binds F-actin with high affinity. Nuclei were stained with Hoechst (Molecular Probes, Life Technologies, USA) and analysed by confocal microscopy (Nikon Eclipse Ti). The semiquantitative analysis of fluorescence intensity was performed using IMAGE-J software (http://rsbweb.nih.gov/ij/) [75].

Immunofluorescence and cell cytoskeleton analysis

HUVEC monolayers were grown to confluence on coverslips coated with type I collagen (Calbiochem, Darmstadt, Germany) and were treated with SW480 and SW620 cell derived

exosomes (20 µg/ml) or low serum medium for 3 and 6h. For SW480 and SW620 cell treatments $1x10^5$ cells were plated. After incubation, cells were processed as described [112]. For HUVEC was used antibody for VE cadherin and ZO-1 (1:100; Santa Cruz Biotechnology, Santa Cruz CA, USA). Cells were stained with Texas Redconjugated secondary anti-mouse antibodies (1:100; Molecular Probe, Eugene, Oregon USA) and analyzed by confocal microscopy (Nikon Eclipse Ti). The semiquantitative analysis of fluorescence intensity was performed using IMAGE-J software (http://rsbweb.nih.gov/ij/) [74].

RNA extraction and real-time PCR

HUVEC cells were grown to confluence in 6-well plates and incubated for 6h with SW480 and SW620 cell derived exosomes (5-10-20 µg/ml). VE-CADHERIN and ZO-1 transcript levels were measured by reverse transcription (RT) and TaqMan real-time quantitative polymerase chain reaction (RT-PCR) and analyzed as described [75]. The following primers were used: VE-CADHERIN, ZO-1 (Applied Biosystems, Foster City, CA, USA). GAPDH was used as the internal control.

FACS analysis of large EVs

Purified large EVs from conditioned media of SW480 and SW620 cells were washed in PBS, fixed and permeabilized with 0.5% Tween 20 and then stained with rabbit monoclonal CK18 (Abcam, 1:50). Samples were processed on a LSRII Flow Cytometer (BD) using 1, 2 and 10

μm bead standards [76, 77]. A minimum of 3000 events per experiment was recorded and the data analysis was performed with the FlowJo software (Treestar). The plot shows the mean fluorescent intensity (MFI). Statistical significance was calculated using a 2-tailed unpaired Student's t test.

Caspases assay

SW480 cells treated for 3-6h with SW480 and SW620 cell derived exosomes were analyzed for activity of caspase 3/7 by Caspase-Glo® 3/7 Assay System (Promega, Mannheim, Germany) according to manufacturer's instructions. Luminescence was recorded using GloMax Multi+microplate reader (Promega, Mannheim, Germany).

Migration and invasion assay

In vitro cancer cell migration and invasion activities were evaluated in transwells as described previously [78]. Cells were treated with increased doses of SW480 and SW620 cell derived exosomes Briefly SW480 and SW620 cells (280 x 10^3/ml) were suspended in serum-free RPMI 1640 medium supplemented with 0.1% BSA, with or without increased amount of exosomes (20-50 μg/ml) in transwell chemotaxis chamber coated with collagene equipped with 8 μm pore filters and exposed to medium supplemented with 10 % of FBS (chemoactractant) and the plates were incubated for 72 h at 37°C in 5% CO_2. For HUVEC (2 x 10^6/ml) treatments the doses of 5-10-20 μg/ml of exosomes have been used and the plates were incubated for 6 h. To analyze colon cancer cell invasion, the transwell insert chambers

were coated with Matrigel. After treatments the cells that did not migrate were removed from the top of the transwell filters by scraping, while the cells that had penetrated the collagene (migration assay) or matrigel (invasion assay) were fixed in ethanol and stained with Diff-Quick (Medion Diagnostics GmbH, Dudingen, Switzerland). Each test group was tested in three independent experiments; the number of migrating cells in five high-power fields per well were counted at 400x magnification.

Adhesion assay

For adhesion assays HUVEC fixed monolayer was incubated for 3 hr with SW480 or SW620 cells pretreated or not with increased amount of exosomes (20-50 µg/ml). Adherent cells were stained with hematoxylin/eosin; each test group was assayed in triplicate; five high power (400X) fields were counted for each condition

Tube formation of HUVEC on Matrigel

Matrigel was used to test the effects of exosomes on in vitro vascular tube formation as described [79]. HUVEC were plated on Matrigel at concentration of 70000 cells/well in endothelial basal medium containing 0.2% of FBS, supplemented with increased amount of exosomes (5-10-20 µg/ml) or EGM as positive control or low serum medium as negative control. Cells were incubated for 4 hr and then evaluated by phase-contrast microscopy and photographed. The length of the cables was measured manually with the IMAGE-J software (http://rsbweb.nih.gov/ij/) [80].

Dextran permeability assay

The permeability of treated HUVEC monolayers grown on 0.4 mm filters was measured by the appearance of FITC-dextran, which was added for 1h to the top well after 3-6-9h of treatment with SW480 and SW620 cell derived exosomes. The absorbance of the CM in the bottom well at 495 nm was compared with the PBS (control) condition. Luminescence was recorded using GloMax Multi+microplate reader (Promega, Mannheim, Germany).

Proteomic analyses: sample preparation, SWATH-MS and data analysis

After isolation and resuspension in PBS, exosomes released by SW480 and SW620 cells were prepared to be analyzed by quantitative mass spectrometry. Exosomes were quantified using the Bradford assay; 200 µg of each sample were subjected to in-solution digestion using 50% 2,2,2-trifluoroethanol (TFE) in PBS, as described previously [81], with some modifications. Briefly, after 2 minutes sonication in an ice bath, exosomes were incubated with constant shaking for 2h at 60°C; extracted exosomal proteins were reduced with 5 mM DTT for 30' at 60°C, alkylated with 25mM IAA for 30' in the dark at room temperature and, after addition of 100 mM ammonium bicarbonate pH 8.0 and 2mM CaCl2, digested for 18 hours with trypsin at a ratio of 1:50 (w/w). Once stopped digestion with formic acid (FA) 90%, extracted peptides were centrifuged at 14000 g for 10 minutes at 4°C and desalted using OMIX C18 Zip-Tip. Peptides were eluted in 70% ACN/H2O (70:30, v/v) containing 0.1% FA, dried and resuspended in 5% ACN/H2O (5:95, v/v) containing 0.1% FA. Peptide concentration was determined with a Nanodrop; before analysis, all samples were diluted to 1 ug/ul. A pool containing equal amount of the two samples has been prepared to generate the spectral reference library for SWATH-MS analysis.

All analyses were performed using a Triple TOF 5600 Plus System (AB Sciex, Framingham, U.S.A.) equipped with an Eksigent ekspert nanoLC 425 system. After being cleaned up and pre-concentrated on a C18 reversed-phase trap column (Reversed Phase Solid Phase Extraction Trap, 20mm, C18, ID 100 um; Nanoseparations) for 10 minutes, employing a mobile phase, from loading pump, containing 2% ACN/H2O (2:98, v/v) in 0.1% TFA, at a flow rate of 5 ul/min, peptides (4ug) were separeted on the C18 analytical column (Standard column packed with 3um Biosphere C18 particles, 200mm, ID 75 um; Nanoseparations) , equilibrated at 40°C with a solvent A (0,1% FA in water), at a flow rate of 300 nL/min, using a 200 min gradient method: (10-28% buffer B over 120 min, 28-60% buffer B over 30 min; 60-95% buffer B over 2 min, hold buffer B at 95% for 10 min, 95-10% buffer B in 2 min and hold buffer B at 10% for remaining 36 min). Buffer B consists of 98% ACN/H2O (98:2, v/v) containing 0.1% FA.

To generate the spectral reference library, the pooled sample was subjected to traditional Information Dependent Acquisition (IDA); the mass spectrometer was operated such that an MS scan (350-1250 m/z; accumulation time 250 ms) analyzed TOF in high resolution mode (>30,000), followed by 25 MS/MS scans (230-1500 m/z, accumulation time 150 ms) analyzing TOF in high sensitivity mode (resolution >15,000) with rolling collision energy. For fragmentation, precursors, with a charges from 2 to 5, were selected if exceeding a threshold of 50 counts per second (cps); former ions were excluded for 15s. The IDA file was submitted to ProteinPilot™ 4.5 software (AB SCIEX, Toronto, Canada) using Uniprot as human protein database. The search was performed with the following settings: identification as sample type, iodoacetamide cysteine alkylation, digestion by trypsin; no special factors; run of false discovery rate analysis; protein pilot score >0.05 with a 10% confidence threshold.

For SWATH acquisition, peptides were analysed in SWATH-MS mode. At a cycle time of 3.3s, 50ms TOF/MS survey scan was performed between 350-1250 Da with 34x25 Da swath. Each SWATH MS/MS acquisition was performed between 230-1500 Da using a 96ms accumulation time. Three replicates were acquired for each sample. The SWATH files were processed by PeakView v2.2 and MarkerView for quantitative and statistical data analysis, respectively. In PeakView they were analyzed using the following parameters: 10 peptides; 7 transitions; peptide confidence threshold of 90%; FDR threshold of 5%; exclusion of modified peptides; XIC Extraction Window of 15 min; XIC width set at 0.05 Da. Protein list with FDR lower than 5% was exported to MarkerView to perform Principal Component Analysis (PCA) and t-test. Volcano Plot graphically display t-test results, plotting Log Fold Change (x axis) vs p-value (y axis).

Gene ontology and pathway analyses were performed using FunRich (http://www.funrich.org) and iPathway Guide (http://www.advaitabio.com/ipathwayguide).

Assay for RhoA activation

Seeding of HUVEC and SW480 cells were preformed as described above. Rho A activity and total Rho A were evaluated at 6 hours after treatment with SW620 cell derived exosomes using a colorimetric Rho A activity and total Rho A assays from Cytoskeleton, Inc. The assay was performed according to the manufacturer's instructions. The absorbance of each sample was measured in triplicate at 490 nm and recorded using a microplate spectrophotometer (Model 680XR, BioRad). Each sample reading was normalized by subtracting the reading from the blank from the sample reading [82].

Statistics

Data were expressed as means ± SEMs of the indicated number of experiments. Statistical analysis was performed by using a unpaired Student's t test. Differences were considered to be significant when P values were < than 0.05.

Results and Discussions

PART I: SW480 and SW620 exosomes characterization

SW480 and SW620 cells release exosomes

Exosomes released by SW480 and SW620 cells into the culture medium after a 24-hr culture period in presence of FBS previously ultracentrifuged (vesicle free media), were characterized on the base of their diameter [Figure 13A] and of the presence of exosome markers [Figure 13B].

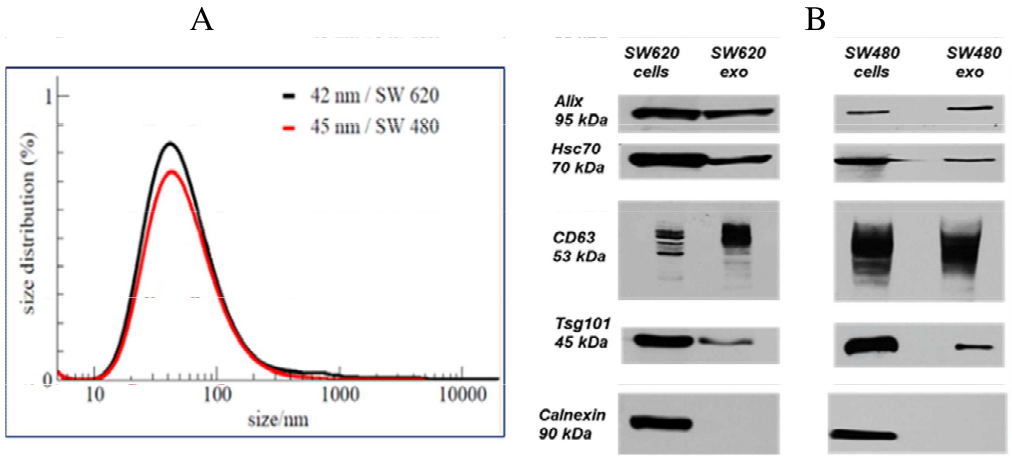

Figure 13: Characterization of exosomes released by SW480 and SW620 cells. A. Dynamic light scattering (DLS) analysis of exosomes isolated from SW620 and SW480 cells shows no differences in the size distribution between two type of exosomes Results were plotted as a % mass distribution in order to accurately represent the size distribution of the biological sample. B. Western blot analysis for Alix, Hsc70, CD63 TSG101 and Calnexin in cell and exosome protein lysates (30 µg).

Proteomic analyses of exosomes released by SW480 and SW620 exosomes

In order to characterize the protein profiling of exosomes derived from SW480 and SW620 cells, a proteomic analysis was performed. A total of 412 proteins have been identified in exosomes, derived from both colon cancer cell lines, and by the FunRich (www.funrich.org) software, they have been classified through cellular component of Gene Ontology (CC-GO) terms. Figure 14 shows that 69% of the identified proteins have been already described as exosomal proteins, 46% are lysosomal proteins, 36% are extracellular proteins, 27% are cytosolic proteins, 16% are cytoskeletal proteins, 23% are centrosome proteins, 19% are mitochondrial proteins, 19% are nuclear proteins and 5,6% are ribosomal proteins.

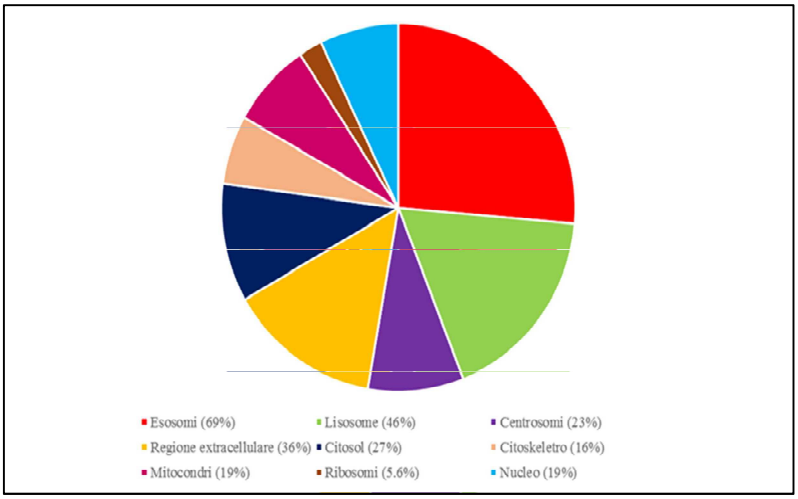

Figure 14: 9 more represented functional classes of cellular component of Gene Ontology terms among identified proteins of SW480 and SW620 exosomes.

SWATH analyses of SW480 and SW620 exosome proteomic profiling

In order to obtain a quantitative proteomic profiling of SW480 and SW620 exosomes a SWATH-MS approach was performed. SWATH analysis is a quantitative label-free method that combines the high specificity of DIA method with a targeted data extraction strategy. Data obtained from SWATH analysis were processed by Peack View 2.2 software and then analyzed by Marker View software that provides an univariate analysis (T-test) and a multivariate analysis (analysis of the main components – PCA). Figure 15 shows a good reproducibility (PC2= 22%) and a significant difference of protein profiling among exosomes derived from SW480 and SW620 cell lines (PC1= 65,9%).

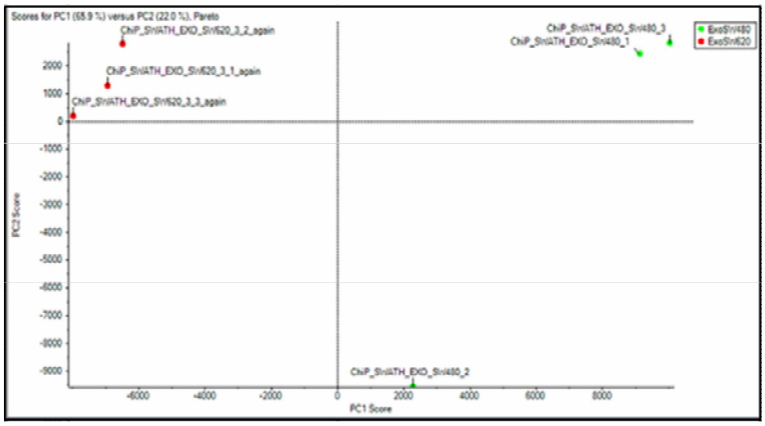

Figure 15: PCA graph: 3 replicates of SW620 exosomes (red) and SW480 exosomes (green).

Volcano plot in Figure 16 shows the different protein distribution of exosomes. Only proteins with a p ≤0.05 and a log10 fold-change >0.2 or <–0.2 (for up-regulated and down-regulated proteins, respectively) were considered for further analysis.

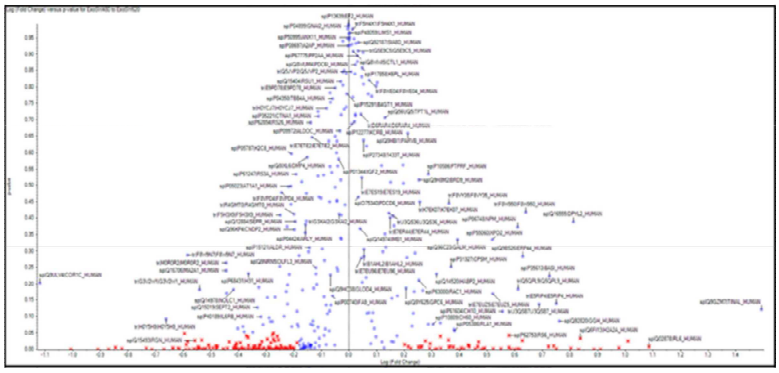

Figure 16: the Volcano plot shows in red SW620 exosomes up-regulated proteins (on the right) and down-regulated proteins (on the left).

In order to characterize SW620 exosome down - and up – regulated proteins, a GO enrichment analysis on all differentially expressed proteins was performed using iPathway Guide (http://www.advaitabio.com/ipathwayguide.html). Figure 17 shows the cellular component (17A) and functional pathways (17B) of up - and down – regulated proteins in SW620 exosomes. The different distribution of SW620 exosome proteins shows an enrichment in exosomal proteins (66%, Figure 17A), cytoskeletal proteins (14,4% Figure 17A) and in tubulin (3,7% Figure 17B) and actin folding involvement proteins (3,7% Figure 17B), on the other hand SW620 exosomes show a lower expression of ribosomal proteins (8%, Figure 17A) and protein involved in translational processes (1,2%, Figure 17B).

A

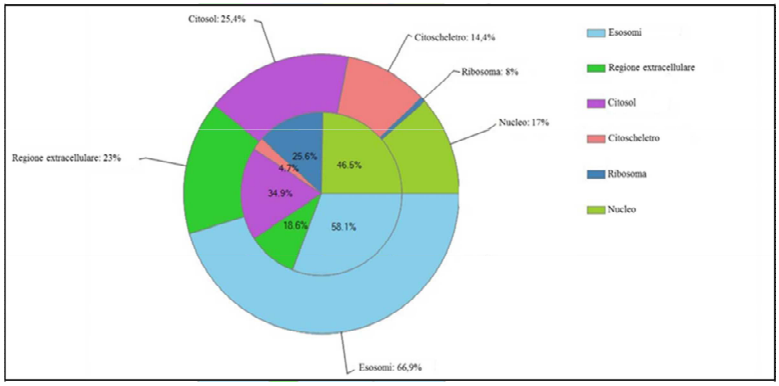

B

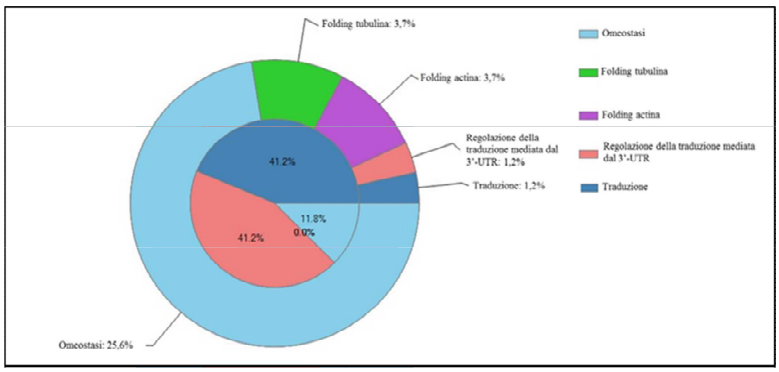

Figure 17: A. Pie chart of 6 more represented functional classes of cellular component of Gene Ontology terms in SW620 exosomes versus SW480 exosomes. The external area of pie chart shows the up-regulated SW620 exosome proteins; the internal area of pie chart shows the down-regulated SW620 exosome proteins. The % shown indicates the total number of proteins of each class among all up – and down – regulated proteins. B. Pie chart of 5 more represented pathways in SW620 exosomes versus SW480 exosomes. The external area of pie chart shows the up-regulated SW620 exosome protein releated patways; the internal area of pie chart shows the down-regulated SW620 exosome protein releated pathways. The % shown indicates the total number of proteins of each class among all up – and down – regulated protein releated patways.

Among the up-regulated SW620 exosome proteins [Table 1] some of these have drawen particularly our attention since they could represent possible mediators of metastatic phenotype. Among them RacGap1 protein has been found to be 10 fold up-regulated in exosomes derived from metastatic cell line. RacGap1 expression was associated, by Imaoka H. et al. [82], to lymph-node metastasis and poor prognosis in CRC, implicating a prognostic

value for RacGap1 during tumor progression. Additionally to the role as biomarker, RacGap1, described also as important GTP-asi Rho A activator protein [83], has been implicated, in melanoma cytoskeletal rearrangement [84]. Furthermore, our analysis have identified other up-regulated SW620 exosome proteins, that have recently been associated with metastasis progression in other systems, such as Transgelin, identified by Rao et al. [85], as a potential biomarker of highly aggressive breast cancer; Flotillin-2, which expression was found to be positively associated with nasopharyngeal carcinoma metastasis [86], and Haptoglobin, involved, in ovarian cancer, in the process of cell migration, through rearrangement of the actin cytoskeleton [87]. Finally Desiniotis A. et al. [88] have shown that the talin protein expression, that was found up-regulated in SW620 exosomes, is significantly increased in prostate cancer compared with benign and normal prostate tissue; moreover its overexpression was correlated with progression to metastatic disease, implicating a prognostic value for talin during tumor progression.

Table 1 - up and down regualted proteins in SW620 exosomes

	AC	Entry name	Protein name	Gene name	p-value	FC Eso620 vs Eso480
1	Q9H0H5	RGAP1_HUMAN	Rac GTPase-activating protein 1	RACGAP1	1,20E-05	10,18091884
2	J3QR68	J3QR68_HUMAN	Haptoglobin	HP	1,02E-06	8,106159216
3	Q9BR76	COR1B_HUMAN	Coronin-1B	CORO1B	0,00065	7,413389614
4	P30566	PUR8_HUMAN	Adenylosuccinate lyase	ADSL	0,00565	7,0136704
5	P08567	PLEK_HUMAN	Pleckstrin (Platelet 47 kDa protein)	PLEK	0,00113	6,652488406
6	P09960	LKHA4_HUMAN	Leukotriene A-4 hydrolase	LTA4H	0,0024	5,407672728
7	J3QLD9	J3QLD9_HUMAN	Flotillin-2 (HCG1998851, isoform CRA_h)	FLOT2	1,23E-05	5,172922076
8	P06858	LIPL_HUMAN	Lipoprotein lipase	LPL	0,0003	4,68383039
9	P04040	CATA_HUMAN	Catalase	CAT	0,00423	4,343156558
10	Q6ZMU1	C3P1_HUMAN	Putative protein C3P1	C3P1	0,00162	4,338468515
11	P25325	THTM_HUMAN	3-mercaptopyruvate sulfurtransferase	MPST	0,0028	4,15815293
12	H3BT58	H3BT58_HUMAN	Coactosin-like protein	COTL1	0,00109	4,114824684
13	E5RGR0	E5RGR0_HUMAN	Acyl-protein thioesterase 1	LYPLA1	0,04835	3,937824646
14	P15169	CBPN_HUMAN	Carboxypeptidase N catalytic chain	CPN1	3,57E-06	3,894046635
15	P02786	TFR1_HUMAN	Transferrin receptor protein 1	TFRC	0,01395	3,87955653
16	J3KQ42	J3KQ42_HUMAN	Tetraspanin	TSPAN4	0,02402	3,848343009
17	P19827	ITIH1_HUMAN	Inter-alpha-trypsin inhibitor heavy chain H1	ITIH1	3,65E-05	3,787190081
18	P21399	ACOC_HUMAN	Cytoplasmic aconitate hydratase (Aconitase)	ACO1	2,43E-05	3,631654484
19	Q15493	RGN_HUMAN	Regucalcin (RC) (Gluconolactonase)	RGN	0,02643	3,620529905
20	P22352	GPX3_HUMAN	Glutathione peroxidase 3 (GPx-3)	GPX3	7,13E-06	3,551767132
21	P04114	APOB_HUMAN	Apolipoprotein B-100 (Apo B-100)	APOB	0,00711	3,509944913
22	E9PBW4	E9PBW4_HUMAN	Hemoglobin subunit gamma-2	HBG2	0,00242	3,491245972
23	P53999	TCP4_HUMAN	Activated RNA polymerase II transcriptional coactivator p15	SUB1	0,02751	3,416909408
24	P30086	PEBP1_HUMAN	Phosphatidylethanolamine-binding protein 1	PEBP1	0,00124	3,416471762
25	B7ZKJ8	B7ZKJ8_HUMAN	ITIH4 protein	ITIH4	0,0002	3,345565708
26	O00299	CLIC1_HUMAN	Chloride intracellular channel protein 1	CLIC1	1,76E-05	3,331807909
27	Q92954	PRG4_HUMAN	Proteoglycan 4	PRG4	0,0131	3,226359588
28	Q99832	TCPH_HUMAN	T-complex protein 1 subunit eta	CCT7	0,0038	3,203673057
29	P35573	GDE_HUMAN	Glycogen debranching enzyme	AGL	0,00387	3,111510199
30	P51857	AK1D1_HUMAN	3-oxo-5-beta-steroid 4-dehydrogenase	AKR1D1	0,00947	3,032371453
31	K7EIK7	K7EIK7_HUMAN	Echinoderm microtubule-associated protein-like 2	EML2	0,00074	3,020299767
32	Q5T6H7	Q5T6H7_HUMAN	Xaa-Pro aminopeptidase 1	XPNPEP1	0,00802	2,995761367
33	P48147	PPCE_HUMAN	Prolyl endopeptidase (PE)	PREP	0,00033	2,852466625
34	P22314	UBA1_HUMAN	Ubiquitin-like modifier-activating enzyme 1	UBA1	6,10E-06	2,848183437
35	P50454	SERPH_HUMAN	Serpin H1	SERPINH1	0,00295	2,759039856
36	C9J9K3	C9J9K3_HUMAN	40S ribosomal protein SA	RPSA	0,02231	2,713036845
37	Q13418	ILK_HUMAN	Integrin-linked protein kinase	ILK	0,0011	2,623350283
38	P06737	PYGL_HUMAN	Glycogen phosphorylase, liver form	PYGL	0,00113	2,610582577
39	Q9H2A2	AL8A1_HUMAN	Aldehyde dehydrogenase family 8 member A1	ALDH8A1	0,00796	2,590344031
40	P08758	ANXA5_HUMAN	Annexin A5	ANXA5	0,00169	2,589428538
41	P10644	KAP0_HUMAN	cAMP-dependent protein kinase type I-alpha regulatory subunit	PRKAR1A	2,09E-05	2,570876139
42	P02794	FRIH_HUMAN	Ferritin heavy chain (Ferritin H subunit)	FTH1	0,01209	2,564376833
43	F5GWF6	F5GWF6_HUMAN	T-complex protein 1 subunit beta	CCT2	0,00159	2,558545799
44	E9PM69	E9PM69_HUMAN	26S protease regulatory subunit 6A	PSMC3	0,01767	2,554449116
45	P01024	CO3_HUMAN	Complement C3	C3	4,05E-05	2,548601432
46	Q93063	EXT2_HUMAN	Exostosin-2	EXT2	2,81E-05	2,49295606
47	Q6EMK4	VASN_HUMAN	Vasorin (Protein slit-like 2)	VASN	5,82E-05	2,48614527
48	P68366	TBA4A_HUMAN	Tubulin alpha-4A chain	TUBA4A	0,00626	2,444021398
49	P05546	HEP2_HUMAN	Heparin cofactor 2	SERPIND1	1,54E-06	2,426340168

	AC	Entry name	Protein name	Gene name	p-value	FC Eso620 vs Eso480
50	O95336	6PGL_HUMAN	6-phosphogluconolactonase	PGLS	0,00123	2,421122953
51	P51884	LUM_HUMAN	Lumican (Keratan sulfate proteoglycan lumican)	LUM	9,01E-05	2,416927236
52	Q9UGM3	DMBT1_HUMAN	Deleted in malignant brain tumors 1 protein	DMBT1	0,00019	2,385287011
53	Q8WZ75	ROBO4_HUMAN	Roundabout homolog 4	ROBO4	0,04121	2,350860746
54	Q9Y240	CLC11_HUMAN	C-type lectin domain family 11 member A	CLEC11A	0,00082	2,327522633
55	Q16401	PSMD5_HUMAN	26S proteasome non-ATPase regulatory subunit 5	PSMD5	0,03623	2,319479283
56	P55263	ADK_HUMAN	Adenosine kinase (AK)	ADK	0,01128	2,313928362
57	P02649	APOE_HUMAN	Apolipoprotein E (Apo-E)	APOE	0,00031	2,294609273
58	P02748	CO9_HUMAN	Complement component C9	C9	5,43E-05	2,262701281
59	P00734	THRB_HUMAN	Prothrombin	F2	0,00027	2,236610672
60	P26038	MOES_HUMAN	Moesin (Membrane-organizing extension spike protein)	MSN	0,00341	2,220988005
61	Q16394	EXT1_HUMAN	Exostosin-1	EXT1	0,00781	2,21620921
62	X6RJP6	X6RJP6_HUMAN	Transgelin-2	TAGLN2	4,85E-05	2,208234338
63	O43505	B3GN1_HUMAN	Beta-1,4-glucuronyltransferase 1	B4GAT1	0,00918	2,182751695
64	P50552	VASP_HUMAN	Vasodilator-stimulated phosphoprotein (VASP)	VASP	0,00012	2,176865718
65	P07437	TBB5_HUMAN	Tubulin beta chain (Tubulin beta-5 chain)	TUBB	1,24E-05	2,173602861
66	P07902	GALT_HUMAN	Galactose-1-phosphate uridylyltransferase	GALT	8,71E-05	2,167940708
67	P00747	PLMN_HUMAN	Plasminogen	PLG	1,90E-05	2,149076925
68	O00571	DDX3X_HUMAN	ATP-dependent RNA helicase DDX3X	DDX3X	0,00479	2,119021064
69	P00488	F13A_HUMAN	Coagulation factor XIII A chain	F13A1	0,01129	2,11349035
70	B5MCZ9	B5MCZ9_HUMAN	Glutaminyl-peptide cyclotransferase	QPCT	5,21E-06	2,108788924
71	Q92626	PXDN_HUMAN	Peroxidasin homolog	PXDN	0,01385	2,094033397
72	P0DMV8/P0I	HS71A_HUMAN/HS7	Heat shock 70 kDa protein 1A/Heat shock 70 kDa protein 1B	SPA1A/HSPA1	0,00011	2,067906389
73	Q71U36	TBA1A_HUMAN	Tubulin alpha-1A chain	TUBA1A	0,02328	2,06771624
74	Q9NR45	SIAS_HUMAN	Sialic acid synthase (N-acetylneuraminate synthase)	NANS	0,00041	2,047960714
75	J3KPM9	J3KPM9_HUMAN	Signal transducer and activator of transcription	STAT1	0,00463	2,041275383
76	P62140	PP1B_HUMAN	Serine/threonine-protein phosphatase PP1-beta catalytic subun	PPP1CB	0,00069	2,038048773
77	G8JLH6	G8JLH6_HUMAN	Tetraspanin	CD9	0,00061	1,993581934
78	E7EUC7	E7EUC7_HUMAN	UTP--glucose-1-phosphate uridylyltransferase	UGP2	0,03111	1,975693117
79	Q15084	PDIA6_HUMAN	Protein disulfide-isomerase A6	PDIA6	0,00065	1,956645143
80	F8W696	F8W696_HUMAN	Apolipoprotein A-I	APOA1	0,00497	1,953330112
81	P04004	VTNC_HUMAN	Vitronectin (VN) (S-protein)	VTN	0,00071	1,950102248
82	Q06828	FMOD_HUMAN	Fibromodulin (FM) (Collagen-binding 59 kDa protein)	FMOD	0,0015	1,940226221
83	P14550	AK1A1_HUMAN	Alcohol dehydrogenase [NADP(+)]	AKR1A1	0,00565	1,938612494
84	Q9Y490	TLN1_HUMAN	Talin-1	TLN1	0,00033	1,937508358
85	O75874	IDHC_HUMAN	Isocitrate dehydrogenase [NADP] cytoplasmic	IDH1	0,00156	1,931493235
86	Q14517	FAT1_HUMAN	Protocadherin Fat 1 (Cadherin family member 7)	FAT1	0,02011	1,917033498
87	G5E977	G5E977_HUMAN	Nicotinate phosphoribosyltransferase	NAPRT	0,00064	1,891819371
88	Q14204	DYHC1_HUMAN	Cytoplasmic dynein 1 heavy chain 1	DYNC1H1	0,00013	1,891088029
89	B0YIW2	B0YIW2_HUMAN	Apolipoprotein C-III (Apolipoprotein C-III variant 1)	APOC3	0,0436	1,889683531
90	J3QSE5	J3QSE5_HUMAN	Phosphatidylcholine-sterol acyltransferase	LCAT	0,00012	1,885009324
91	E9PCA1	E9PCA1_HUMAN	T-complex protein 1 subunit epsilon	CCT5	0,03155	1,881097793
92	Q01518	CAP1_HUMAN	Adenylyl cyclase-associated protein 1 (CAP 1)	CAP1	0,04922	1,87866143
93	P06733	ENOA_HUMAN	Alpha-enolase (Phosphopyruvate hydratase)	ENO1	5,19E-05	1,870794374
94	G3V1D3	G3V1D3_HUMAN	Dipeptidyl peptidase 3	DPP3	0,02461	1,859367173
95	P18669	PGAM1_HUMAN	Phosphoglycerate mutase 1	PGAM1	0,00059	1,846476794
96	P35858	ALS_HUMAN	Insulin-like growth factor-binding protein complex	IGFALS	0,00727	1,829651646
97	P12259	FA5_HUMAN	Coagulation factor V	F5	7,57E-06	1,826821903
98	I3L145	I3L145_HUMAN	Sex hormone-binding globulin	SHBG	0,00189	1,824845778

	AC	Entry name	Protein name	Gene name	p-value	FC Eso620 vs Eso480
99	P63104	1433Z_HUMAN	14-3-3 protein zeta/delta	YWHAZ	0,03915	1,821984128
100	Q12860	CNTN1_HUMAN	Contactin-1	CNTN1	0,00054	1,805755409
101	P61224	RAP1B_HUMAN	Ras-related protein Rap-1b (GTP-binding protein smg p21B)	RAP1B	0,00015	1,804708544
102	P62937	PPIA_HUMAN	Peptidyl-prolyl cis-trans isomerase A	PPIA	0,00014	1,798201466
103	Q16473	TENXA_HUMAN	Putative tenascin-XA (TN-XA)	TNXA	0,02789	1,797997874
104	P12955	PEPD_HUMAN	Xaa-Pro dipeptidase (X-Pro dipeptidase)	PEPD	0,00017	1,790661771
105	P00558	PGK1_HUMAN	Phosphoglycerate kinase 1	PGK1	0,0007	1,788335228
106	Q96PD5	PGRP2_HUMAN	N-acetylmuramoyl-L-alanine amidase	PGLYRP2	0,00011	1,775425645
107	P31939	PUR9_HUMAN	Bifunctional purine biosynthesis protein PURH	ATIC	0,01166	1,766114415
108	Q02241	KIF23_HUMAN	Kinesin-like protein KIF23	KIF23	0,00462	1,742602384
109	P51149	RAB7A_HUMAN	Ras-related protein Rab-7a	RAB7A	0,00242	1,724919531
110	O14786	NRP1_HUMAN	Neuropilin-1	NRP1	1,76E-05	1,724080751
111	J3KQE5	J3KQE5_HUMAN	GTP-binding nuclear protein Ran	RAN	0,00488	1,692743574
112	P00338	LDHA_HUMAN	L-lactate dehydrogenase A chain	LDHA	0,00212	1,691314803
113	Q08380	LG3BP_HUMAN	Galectin-3-binding protein	LGALS3BP	0,00046	1,66912085
114	P01008	ANT3_HUMAN	Antithrombin-III (ATIII) (Serpin C1)	SERPINC1	0,00035	1,665623015
115	P35579	MYH9_HUMAN	Myosin-9 (Cellular myosin heavy chain, type A)	MYH9	0,00037	1,662199486
116	O75955	FLOT1_HUMAN	Flotillin-1	FLOT1	0,00947	1,631186678
117	P00742	FA10_HUMAN	Coagulation factor X	F10	0,00359	1,625604629
118	P11021	GRP78_HUMAN	78 kDa glucose-regulated protein (GRP-78)	HSPA5	0,00123	1,621092074
119	H0YCY8	H0YCY8_HUMAN	Dipeptidyl peptidase 1	CTSC	0,00371	1,591427558
120	O00560	SDCB1_HUMAN	Syntenin-1 (Melanoma differentiation-associated protein 9)	SDCBP	0,00219	1,579690449
121	P04406	G3P_HUMAN	Glyceraldehyde-3-phosphate dehydrogenase	GAPDH	0,01952	1,54471304
122	Q02878	RL6_HUMAN	60S ribosomal protein L6 (Neoplasm-related protein C140)	RPL6	0,00783	-12,19498254
123	P62917	RL8_HUMAN	60S ribosomal protein L8	RPL8	0,02471	-10,23333665
124	M0QYS1	M0QYS1_HUMAN	60S ribosomal protein L13a	RPL13A	0,00352	-9,470843278
125	P23527	H2B1O_HUMAN	Histone H2B type 1-O (Histone H2B.2)	HIST1H2BO	0,00011	-8,138833987
126	P62805	H4_HUMAN	Histone H4	HIST1H4A	0,00015	-7,704103145
127	Q6FI13	H2A2A_HUMAN	Histone H2A type 2-A	HIST2H2AA3	0,03397	-6,872346929
128	P04083	ANXA1_HUMAN	Annexin A1	ANXA1	0,00057	-6,781783998
129	Q9NR30	DDX21_HUMAN	Nucleolar RNA helicase 2	DDX21	0,00351	-6,360196424
130	P02765	FETUA_HUMAN	Alpha-2-HS-glycoprotein	AHSG	0,00082	-5,620193637
131	P01116	RASK_HUMAN	GTPase KRas	KRAS	0,00939	-5,500674823
132	P00450	CERU_HUMAN	Ceruloplasmin	CP	0,02695	-4,2339783
133	P39023	RL3_HUMAN	60S ribosomal protein L3	RPL3	0,00047	-4,154895267
134	P18124	RL7_HUMAN	60S ribosomal protein L7	RPL7	0,00072	-4,072392129
135	Q5JR95	Q5JR95_HUMAN	40S ribosomal protein S8	RPS8	0,0002	-3,977041233
136	P02787	TRFE_HUMAN	Serotransferrin (Transferrin)	TF	0,00026	-3,852579659
137	P62753	RS6_HUMAN	40S ribosomal protein S6	RPS6	0,04257	-3,800640782
138	J3QS96	J3QS96_HUMAN	60S ribosomal protein L17 (Fragment)	RPL17	0,00566	-3,800481023
139	P62424	RL7A_HUMAN	60S ribosomal protein L7a	RPL7A	0,00143	-3,539169837
140	P24821	TENA_HUMAN	Tenascin (TN) (Cytotactin)	TNC	0,00142	-3,32865565
141	P50914	RL14_HUMAN	60S ribosomal protein L14 (CAG-ISL 7)	RPL14	0,00138	-3,076010912
142	E9PQD7	E9PQD7_HUMAN	40S ribosomal protein S2	RPS2	0,00061	-3,014848926
143	P61313	RL15_HUMAN	60S ribosomal protein L15	RPL15	0,023	-2,947052917
144	P84103	SRSF3_HUMAN	Serine/arginine-rich splicing factor 3	SRSF3	0,00818	-2,917968117
145	H7BY16	H7BY16_HUMAN	Nucleolin	NCL	0,00188	-2,860375919
146	P36578	RL4_HUMAN	60S ribosomal protein L4	RPL4	0,0087	-2,722305576
147	P23229	ITA6_HUMAN	Integrin alpha-6	ITGA6	0,01271	-2,700700031

	AC	Entry name	Protein name	Gene name	p-value	FC Eso620 vs Eso480
148	P02751	FINC_HUMAN	Fibronectin (FN)	FN1	0,00071	-2,607692964
149	Q00839	HNRPU_HUMAN	Heterogeneous nuclear ribonucleoprotein U	HNRNPU	0,00364	-2,549368094
150	Q13103	SPP24_HUMAN	Secreted phosphoprotein 24	SPP2	0,00035	-2,540371441
151	J3QQ67	J3QQ67_HUMAN	60S ribosomal protein L18	RPL18	2,03E-05	-2,469100506
152	P22466	GALA_HUMAN	Galanin peptides	GAL	0,00767	-2,386958315
153	O75367	H2AY_HUMAN	Core histone macro-H2A.1 (Histone macroH2A1)	H2AFY	0,00778	-2,325741109
154	P02461	CO3A1_HUMAN	Collagen alpha-1(III) chain	COL3A1	0,00706	-2,295462462
155	Q14314	FGL2_HUMAN	Fibroleukin (Fibrinogen-like protein 2)	FGL2	0,02752	-2,291090327
156	P08123	CO1A2_HUMAN	Collagen alpha-2(I) chain (Alpha-2 type I collagen)	COL1A2	0,00229	-2,148766323
157	Q03692	COAA1_HUMAN	Collagen alpha-1(X) chain	COL10A1	0,03998	-2,139668534
158	E7ETH0	E7ETH0_HUMAN	Complement factor I	CFI	0,00204	-2,082309464
159	M0QXM4	M0QXM4_HUMAN	Amino acid transporter	SLC1A5	5,12E-06	-2,042505766
160	P43652	AFAM_HUMAN	Afamin (Alpha-albumin)	AFM	0,0167	-1,963376956
161	P39060	COIA1_HUMAN	Collagen alpha-1(XVIII) chain	COL18A1	0,00215	-1,959142408
162	Q15582	BGH3_HUMAN	Transforming growth factor-beta-induced protein ig-h3	TGFBI	0,02522	-1,88948839
163	Q15063	POSTN_HUMAN	Periostin (PN)	POSTN	0,00878	-1,837109664
164	B0YJC4	B0YJC4_HUMAN	Vimentin (Vimentin variant 3)	VIM	0,00728	-1,815400942
165	B3KSH1	B3KSH1_HUMAN	Eukaryotic translation initiation factor 3 subunit F	EIF3F	0,00771	-1,786117647
166	P19823	ITIH2_HUMAN	Inter-alpha-trypsin inhibitor heavy chain H2	ITIH2	0,00342	-1,670903491
167	P20908	CO5A1_HUMAN	Collagen alpha-1(V) chain	COL5A1	0,00805	-1,639613143

AC:access number to Uniprot database (www.uniprot.otg); Entry name: name to enter to Uniprot; p value is calculataed by T-test; FC shows the proteins modulation of SW620 and SW480 exosomes obtained by quantitative SWATH-analysis. In red up regualted proteins are shown; in gree down regulated proteins are shown AC: numero d'accesso alla banca dati Uniprot(www.uniprot.org); Entry name: nome d'accesso alla banca dati; p-value: calcolato applicando il T-test; FC: indica la modulazione delle proteine negli esosomi620 vs 480 ricavata dall'analisi quantitativa SWATH. In rosso le proteine upregolate negli esosomi620, in verde le downregolate.

PART II: Metastatic cells are able to modulate the phenotype of non metastatic ones through exosomes

The metastatic cell line shows a more aggressive phenotype

SW480 (non metastatic cell line) and SW620 cells (metastatic cell line) have different morphology in culture. Confocal microscopy [Figure 18A] shows that most of the SW480 cells have a spreading, epithelial-type morphology when growing on tissue culture plastic and tend to form multicellular aggregates by 2 days. In contrast, SW620 cells display a more aggressive phenotype showing an ovoid to elongated morphology and form smaller aggregates [Figure 18B].

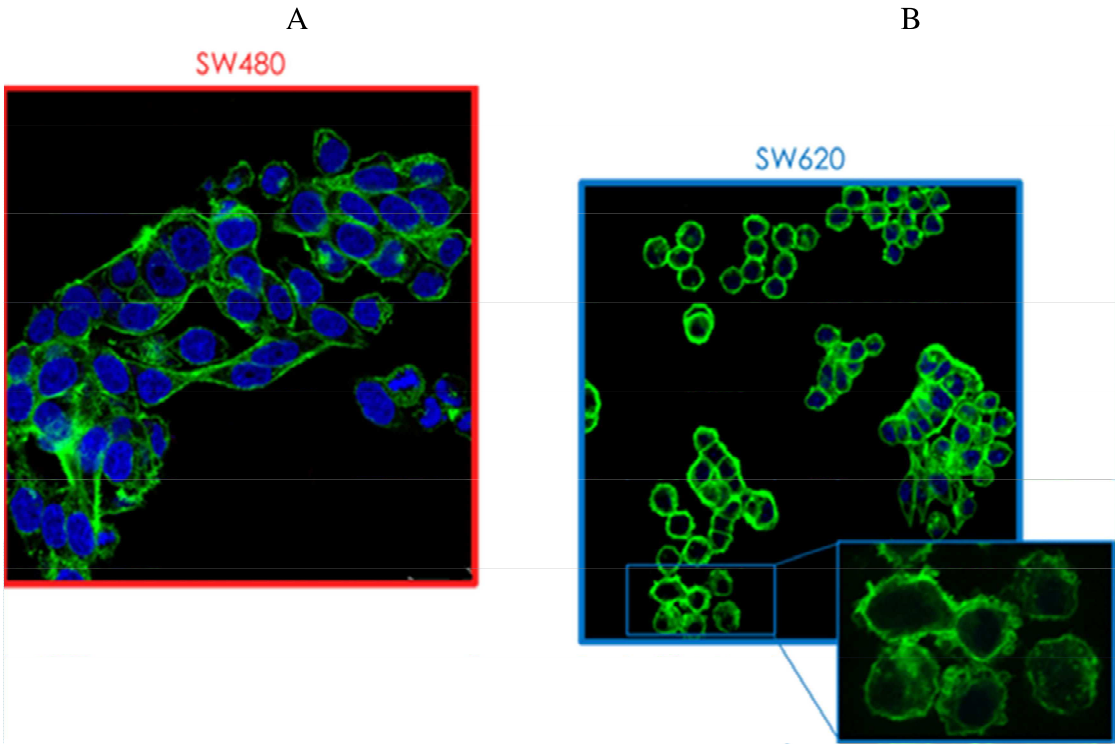

Figure 18: SW620 cells show a more aggressive phenotype. By confocal microscopy, SW480 cells (A) can be seen to have a spreading, epithelial-type morphology and to form cohesive groups, while SW620 cells (B) have

an amoeboid phenotype. Cancer cells are stained with actin green (green), nuclear counterstaining are performed using Hoescht (blue).

This morphology indicates that SW620 cells show membrane blebs typical of amoeboid cells [76]. It has been believed for a long time that blebbing is a morphological feature of apoptosis [89], but during recent decades many data have been collected showing that bleb formation can be the basis for a very special type of cell motility, called amoeboid motility [76, 77, 90]. Amoeboid motility is due to bleb formation that are similar to moving amoebae Dictyostelium discoideum and Entamoeba histolytica in shape (rounded) [91, 92]. Moreover amoeboid behavior is less understood in molecular terms than mesenchymal motility; however, some evidences indicate that this type of cell migration is driven by activation of Rho A or its effector ROCK [94]. It is known that the amoeboid migration is less dependent on pericellular proteolysis and amoeboid cells can migrate rapidly through complex matrices by prominent bleb-like protrusions.

Amoeboid colon cancer cells show more release of large extracellular vesicles

The group of Di Vizio et al. [44, 77, 93 -95] have shown that the tumor cells that exhibit the amoeboid feature of membrane blebbing could release large plasma membrane-derived vesicles (0.5-10 µm) into the extracellular vesicles space. These large extracellular vesicles, are known large oncosomes (LO) because of their atypically large size, because they seem to contain oncogenic material and because they appear to be cancer-specific. On the light of this, the amoeboid cells may be associated with tumor progression, not only as a function of their adaptive plasticity, but also through oncosome-mediated progressive remodeling of their surroundings.

Since the SW620 cell line has a more aggressive phenotype characterized by membrane blebbing, in order to understand if it produces more large oncosomes than the non metastatic cells, we decided to isolate and characterize these vesicles.

In order to determine the buoyant density of large and nano-sized EVs, we used iodixanol (OptiPrep), a medium that is less viscous than sucrose and therefore more likely to enhance the separation of EV populations with differing densities. Large and nano-sized EV pellets, normalized to the same number of cells were separated by flotation in discontinuous 5-60% OptiPrep density gradients following deposition of the EV material at the bottom of the tubes. Western blot analysis of 15 μg of protein lysate [Figure 19A] obtained from the gradient fractions derived from the 100,000 x g pellets of conditioned medium of SW480 and SW620 cells, revealed a population of EVs expressing typical exosome markers, such as CD81 and CD63, which were detected at a buoyant density of 1.10 g/ml and 1.15 g/ml. Western blot analysis of gradient fractions derived from the 10,000 x g pellets of conditioned medium of SW620 cells demonstrated that CK18, identified as potential large EV markers in prostate cancer cell line [93], have floated at buoyant densities of 1.15 g/ml. Levels of large oncosomes marker in EVs derived from SW480 cell line was negligible.

The Figures 19B-C show the right fractions in which is possible to find the exosome and large oncosome populations.

Once we validated the enrichment of CK18 in LO by western blotting, we attempted to quantify LO shedding from both cell lines by measuring the number of CK18 positive LO by FACS [Figure 19D]. We observed that large oncosomes derived from more aggressive cell line show an higher level of CK 18 relative fluorescence intensity than EVs derived from non metastatic ones.

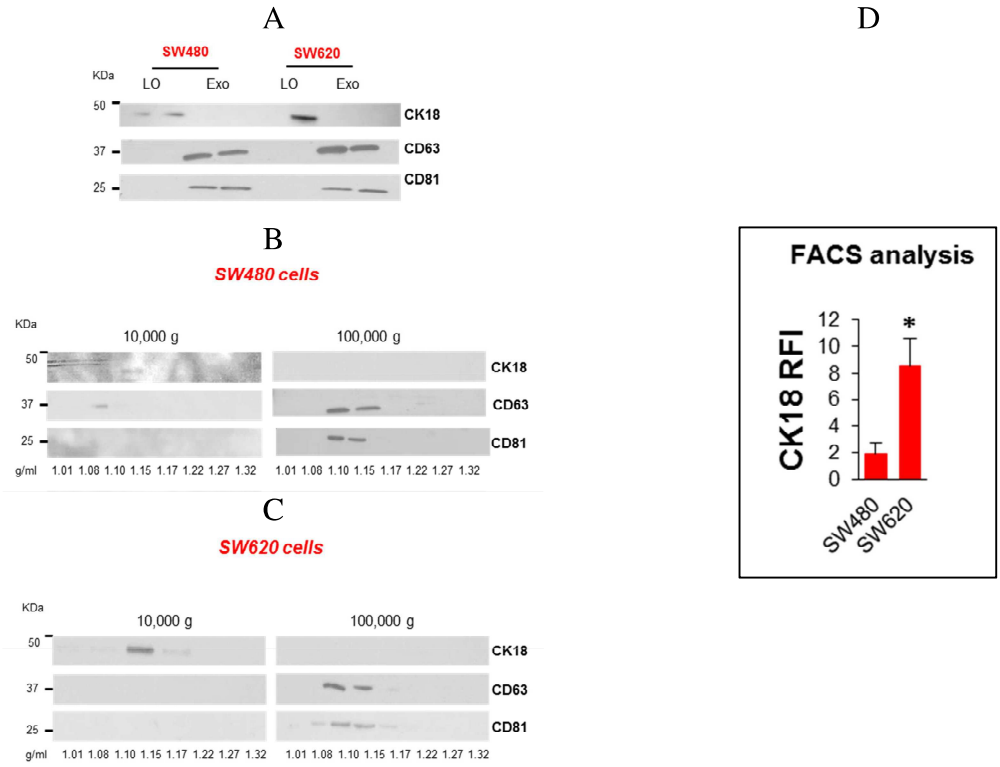

Figure 19: SW620 cells release more large oncosomes than SW480 cell line. A. Western blot of protein lysates from large oncosomes and exosomes were blotted with the indicated antibodies. CD81 and CD63 were expressed specifically in exosomes, and CK18 in large oncosomes. Large oncosomes derived from SW620 cell line show an higher level of CK18 in comparison to the large extracellular vesicles derived from SW480 cell line; the expression level for exosomes is comparable between the two cell lines. B-C. Equal amounts of volumes (20 µl) from OptiPrep fractions (1-8) of EVs derived from SW480 (B) and SW620 (C) were blotted with the indicated antibodies. Exosomes markers CD63 and CD81 were identified in fraction 3 and 4 of both cell lines, corresponding to the buoyant density of 1.10 and 1.15 g/ml. Large oncosomes marker CK18 was identified in fractions 4 of LO derived from SW620 cells, corresponding to the buoyant density of 1.15 g/ml. D. Flow-cytometry (FACS) was used to quantify EVs in the size range of LO, and reveals a significantly higher number of EVs > 1 µm in media from SW620 cells versus SW480 cells. FACS analysis is the mean of 3 independent experiments, *$p < 0.05$.

The treatment with SW620 exosomes induces an amoeboid phenotype in SW480 cells

SW480 cells, treated with their own exosomes or treated with exosomes derived from metastatic cell line, are able to internalize the vesicles. Exosomes rapidly entered into the SW480 cells at 37°C after 3 hours of incubation [Figure 20A].

Morphological analysis of SW480 internalizing SW620 exosomes, shows that exosomes derived from metastatic cell line are able to induce the more aggressive phenotype, typical of SW620 cells, in less aggressive ones. The confocal analysis displays that the treatment of SW480 cells with SW620 exosomes results in a mesenchymal–amoeboid transition (MAT), showing highly dynamic membrane protrusions [Figure 20A-B] and rounded cells.

In particular only the treatment with 20 µg/ml of exosomes, derived from metastatic cell line is able to induce a non apoptotic membrane blebbing [Figure 20C] in non metastatic cells. It is important to underline that there is not the same effect after treatment with exosomes derived from SW480 cells.

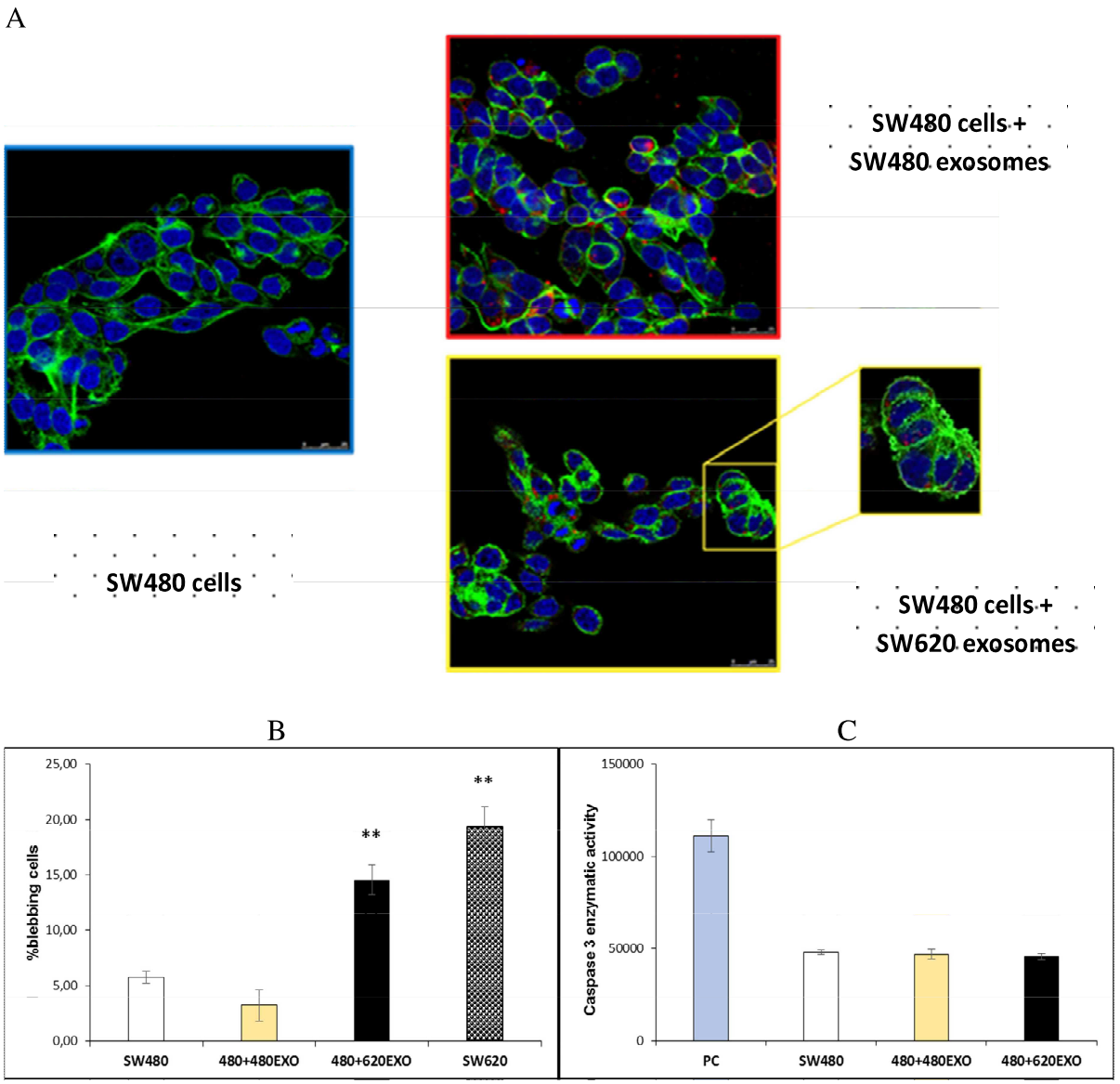

Figure 20: The uptake of SW620 exosomes by SW480 cells induce a non apoptotic membrane blebbing. A The confocal analysis shows that only the treatment with exosomes derived from SW620 cell line is able to induce membrane blebbing in non metastatic ones. The treatment with their own exosomes is not able to influence blebbing in SW480 cells. Cancer cells are stained with actin green (green), nuclear counter staining are performed using Hoescht (blue), exosomes (red) are labeled with PKH26. The figure B shows the % of blebbing cells in both colon cancer cells after exosome treatments and in control condition. The % of blebbing cells were obtained by counting 10 different fields for each conditions. C Enzymatic activity assay shows that the treatment of SW480 cells with exosomes derived from both cell lines does not induce the enzymatic activity of caspase 3.

Exosomes derived from more aggressive cells increase the adhesion of less aggressive ones to endothelial monolayer

While colon cancer progresses, tumor cells adhere to endothelial cells to infiltrate and colonize ectopic tissues. Figure 21 shows the ability of SW620 exosomes to increase the adhesion capacity of SW480 cells on HUVECs.

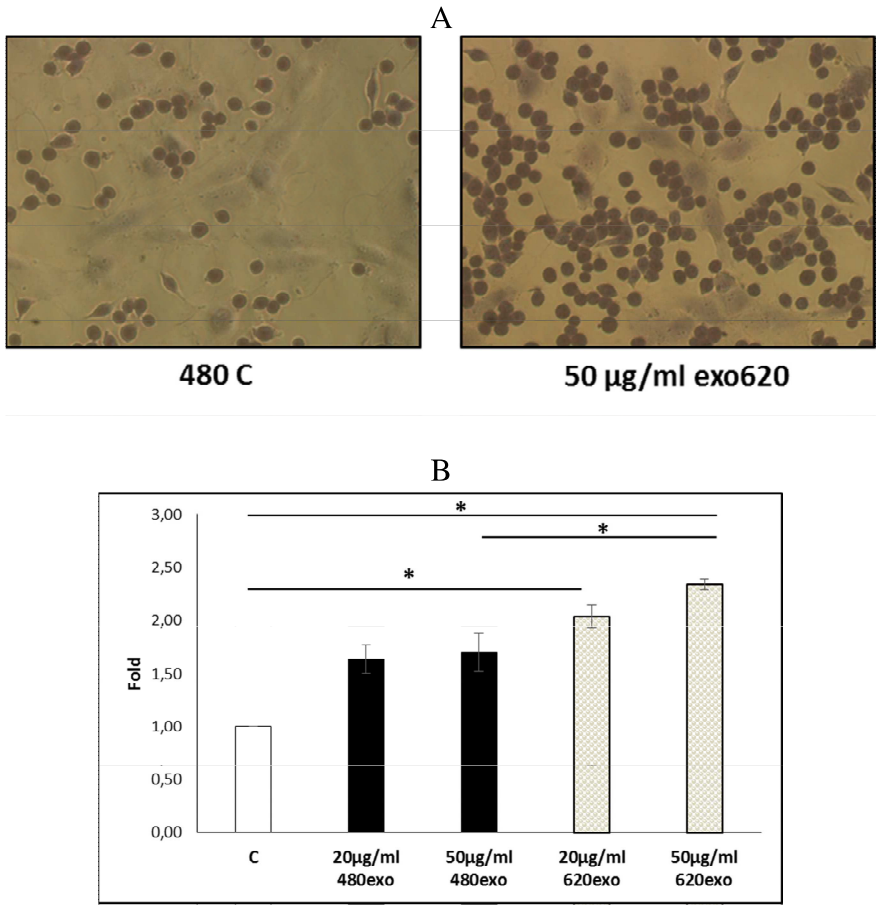

Figure 21: Adhesion of pretreated SW480 cells to HUVEC monolayer: A. Representative images of adherent SW480 cells observed at contrast phase microscopy. C:control with low serum media B. The cells were pretreated for 12 hours with increasing amount of their own exosomes or with exosomes derived from metastatic cell line. Values are the mean ± SD of 5 fields in three independent experiments *$p < 0.05$.

Exosomes derived from more aggressive cells support migratory and invasive ability of less aggressive ones

To evaluate the ability of exosomes derived from highly metastatic cells to propagate their malignant behavior to less aggressive cells, we performed migratory and invasive *in vitro* functional assays. Figure 22 shows that SW620 exosomes are able to increase migration (Figure 22A-B) and invasion (Figure 22C-D) of non metastatic cells more than SW480 exosomes.

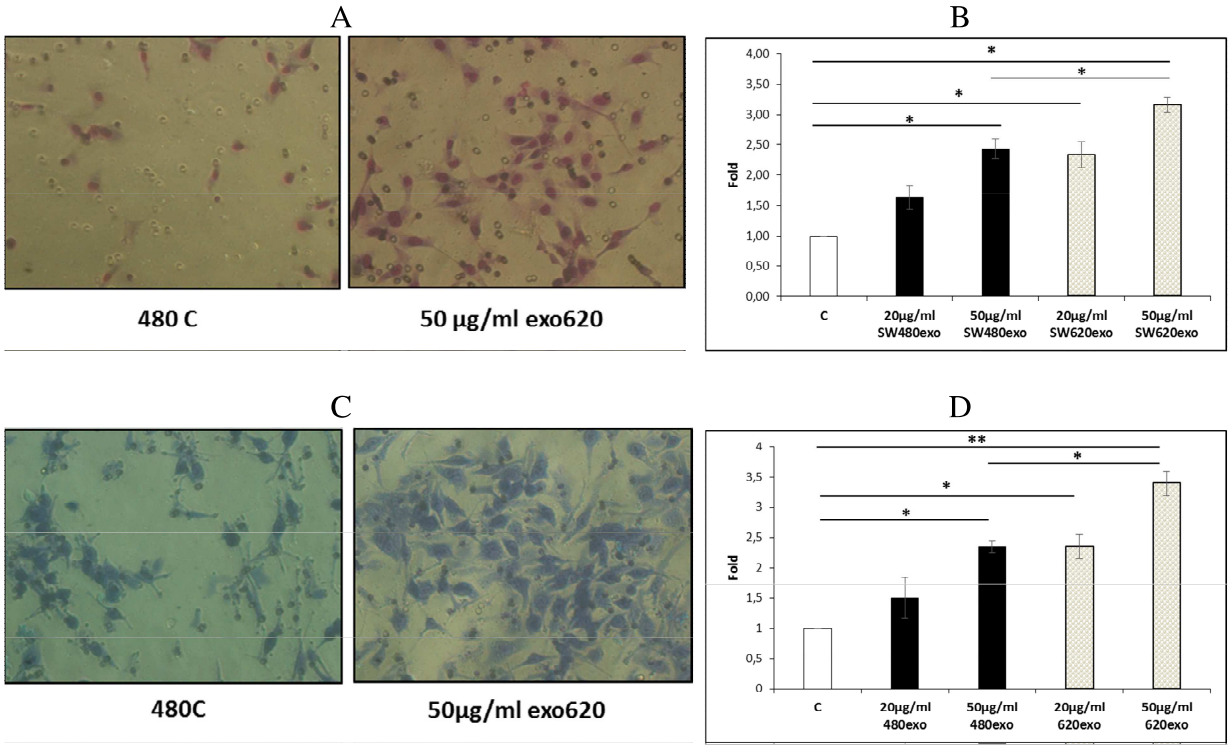

Figure 22: Migration (22A-B) and invasion (22C-D) of SW480 cells treated with exosomes. A. Representative images of migrated SW480 cells observed at contrast phase microscopy. C:control with low serum media B. Migration of SW480 cells treated for 72 hours with increasing amount of their own exosomes or with exosomes derived from metastatic cell line. C. Representative images of invaded SW480 cells observed at contrast phase microscopy. C:control with low serum media D. Invasion of SW480 cells treated for 72 hours with increasing amount of their own exosomes or with exosomes derived from metastatic cell line. Values are the mean ± SD of 5 fields in three independent experiments *$p < 0.05$, **$p < 0.02$.

Exosomes derived from more aggressive cells modulate SW480 phenotype by activating Rho A pathway

In order to understand the molecular mechanism that could explain the morphological and functional effects due to the SW620 exosome treatments, a deep analysis of SW620 exosomes proteomic profiling was performed. As previously mentioned, among SW620 exosome up-regulated proteins in comparison to exosomes derived from non metastatic cells, RacGap1 was found to be of 10 fold up-regulated [Table 1]. Since this protein is described as an important activator of Rho A GTP-ase protein [83], whose activation drives the amoeboid behavior [94], RacGap1 could represent the possible molecular mediator of metastatic phenotype observed in target cells. In order to test if SW620 exosome treatments causes the activation of Rho A pathway, we examined the level of GTP-Rho A activity, the upstream regulator of Rho kinase. Figure 23 shows that the treatment of SW480 cells with SW620 exosomes induce an increase in Rho A activity [Figure 23A], while the level of total protein does not change [Figure 23B].

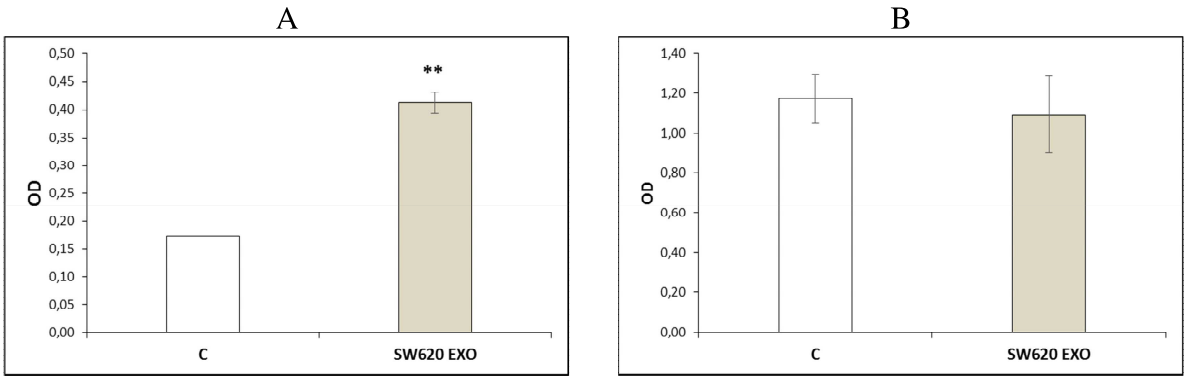

Figure 23: SW620 exosomes activate Rho A pathway. A. After 6 hours of treatment with 20 µg/ml of SW620 exosomes, the level of Rho A activity in SW480 cells increases as compared with the basal level. B. In the same condition of treatment the level of total Rho A does not change. Values are the mean of three independent experiments **$p < 0.02$.

This result confirms our hypothesis that SW620 exosomes modulate SW480 phenotype by activating Rho A pathway involved in the regulation of amoeboid behavior.

PART III: Metastatic cancer derived exosomes modulate junctional component of endothelial barrier

In order to understand how exosomes derived from highly metastatic cells could propagate their malignant behavior, not only to less aggressive cells, but also to other cellular component of the tumor microenvironment, we analyzed the effect of exosomes on endothelial cells.

SW620 exosomes internalized by HUVECs increase endothelial barrier permeability

The ability of SW exosomes to be transferred to endothelial cells is studied by examining the uptake of isolated exosomes labeled with PKH-26 [Figure 24]. HUVECs treated with SW480 and SW620 exosomes internalize the vesicles. Exosomes rapidly enter into the HUVECs at 37°C and localize in the perinuclear compartment after 3 hours of incubation.

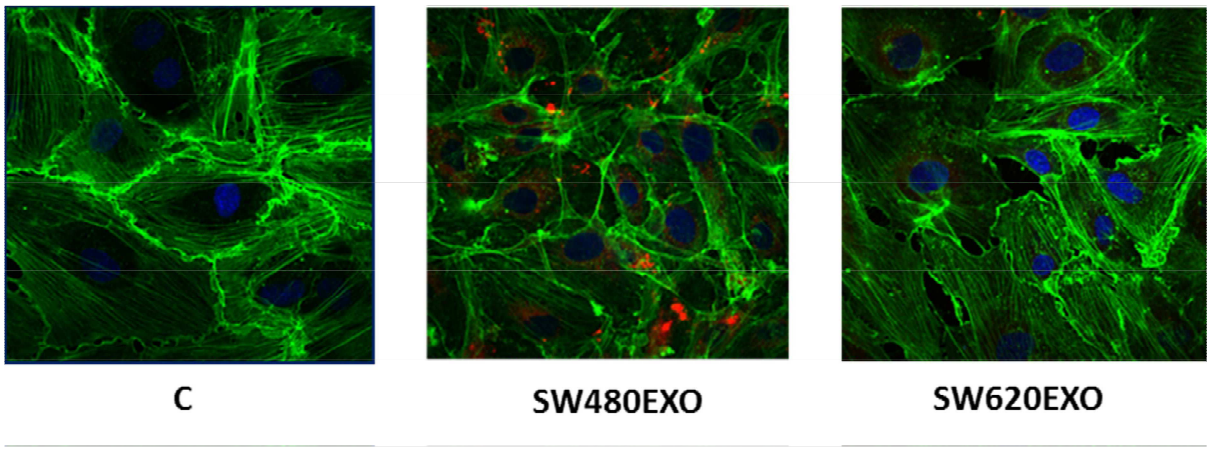

Figure 24: HUVECs internalize SW exosomes. Analysis at confocal microscopy of HUVECs treated, for 3 hours, with 20 µg/ml of SW480 and SW620 exosomes, compared with untreated HUVECs (Control). HUVECs

are stained with actin green (green), nuclear counterstaining are performed using Hoescht (blue), exosomes are labelled with PKH26 (red). The arrows indicate alteration in cell-cell contacts.

Vascular endothelial cells function as a barrier between blood and interstitial compartments. By analyzing HUVECs after 3 hours of SW620 exosome treatments the barrier function of endothelial monolayer seem to be altered. Since enhanced vascular permeability could increase cancer cell dissemination and growth at distant sites, the effect of exosome treatments for a longer time on endothelial barrier stability was evaluated. Figure 25 shows that, the treatment of 6 hours with SW620 exosomes changes microvascular endothelial cell morphology that appears more elongated compared to control and treatment with SW480 exosomes; moreover the integrity of the monolayer was altered due to the separation of cell–cell contacts.

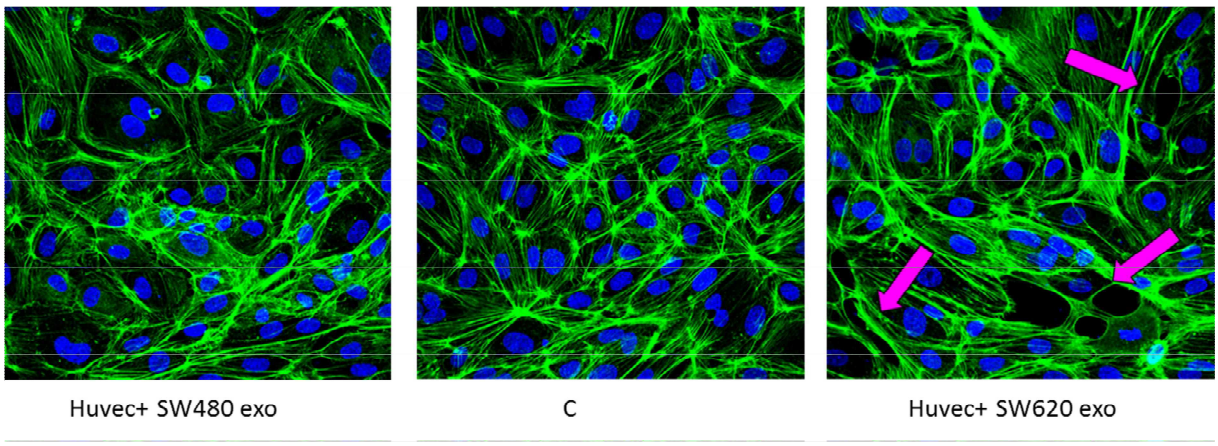

Figure 25: SW620 exosomes alter the integrity of HUVECs monolayer. Analysis at confocal microscopy of HUVECs treated, for 6 hours, with 20 µg/ml of SW480 and SW620 exosomes, compared with untreated HUVECs (C). HUVECs are stained with actin green (green), nuclear counterstaining are performed using Hoescht (blue). The arrows indicate the alteration in cell-cell contacts.

To better evaluate the effect of SW620 exosomes on endothelial barrier, we next performed an in vitro permeability assay by measuring the traversing of dextran-Fitc through HUVECs

monolayers growing on 0.4-µm filters. This assay allows us to understand whether there is an alteration of the monolayer, since the dextran size is 70KDa, only in the presence of an alterated monolayer the passage of the fluorescent probes from the top to the bottom wells can occur. Consistent with the immunofluorescence results, figure 26 shows that only the treatment with SW620 exosomes [Figure 26A] induces, in a time dependent manner [Figure 26B], the passage of the fluorescent probes from top to the bottom wells.

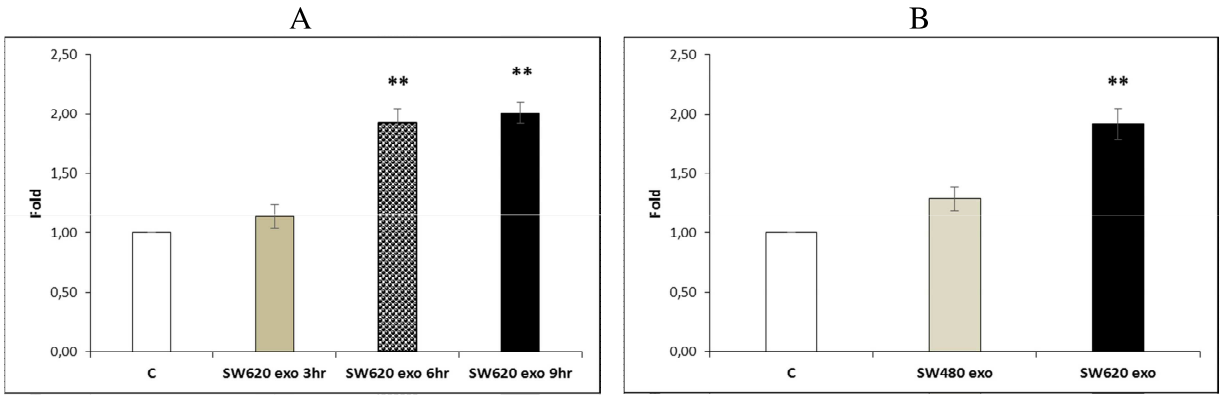

Figure 26: SW620 exosomes induce permeability of HUVECs monolayer in a time dependent manner. A. The permeability of treated HUVECs monolayers grown on 0.4-µm filters was measured by the appearance of dextran-Fitc, which was added to the top well after treatment. The absorbance at 590 nm was compared to the PBS control (C) condition and fold change is shown. A. The permeability of HUVECs monolayers was evaluated after 6 hours of SW480 and SW620 exosome treatments. B. The permeability of HUVECs monolayers was evaluated after 3, 6 and 9 hours of SW620 exosome treatments. Values are the mean of three independent experiments *$p < 0.05$, **$p < 0.02$.

SW620 exosome treatments alter cell-junction component localizations

To investigate the molecular cause leading to endothelial monolayer permeability, we next evaluated the effect of colon cancer exosomes on ZO-1 mRNA expression level, a tight

junctions component, and Ve-cadherin, located at adherens junctions. As shown by RT-PCR results in Figure 27, the treatments with SW exosomes do not affect the expression level of ZO-1 [Figure 27A], and Ve-cadherin [Figure 27B].

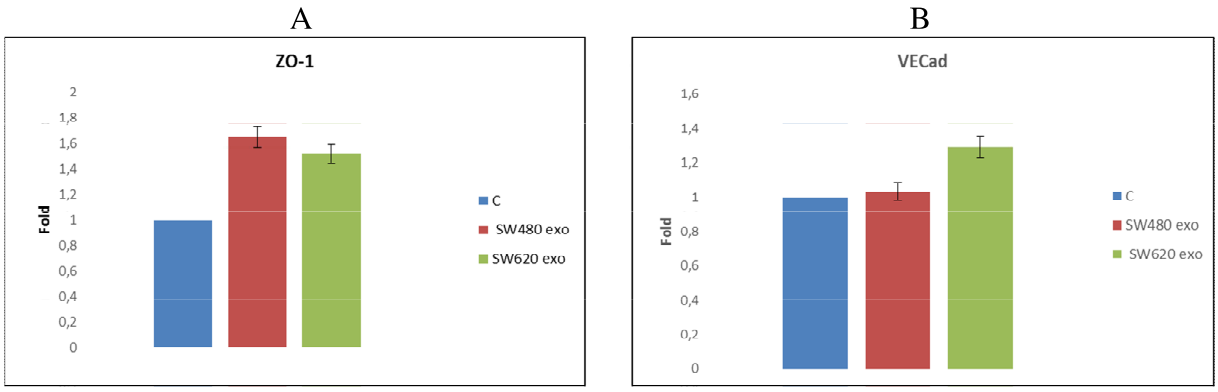

Fig. 27: SW exosomes do not affect the mRNA expression level of ZO-1 (A) and Ve-cadherin (B). HUVECs have been treated with 20 µg/ml of SW exosomes, for 6 hours.

Since data in literature [96-98], have shown a role of cell junction component abnormal distributions in the regulation of endothelial barrier permeability, we tested cell junctional component localizations in HUVECs treated with SW exosomes. As shown in figure 28 and 29 endothelial cells treated with exosomes derived from SW620 cells show a delocalization of ZO-1 [Figure 28], and Ve-cadherin [Figure 29]. ZO-1 and VE-cadherin stainings decrease in intensity and became patchy at the membrane, along with the appearance of a granular cytoplasmic staining in HUVECS treated with 20 µg/ml of SW620 exosomes, compared to control and HUVECs treated with SW480 exosomes, that show continuous peripheral ZO-1 [Figure 28], and VE-cadherin [Figure 29] staining.

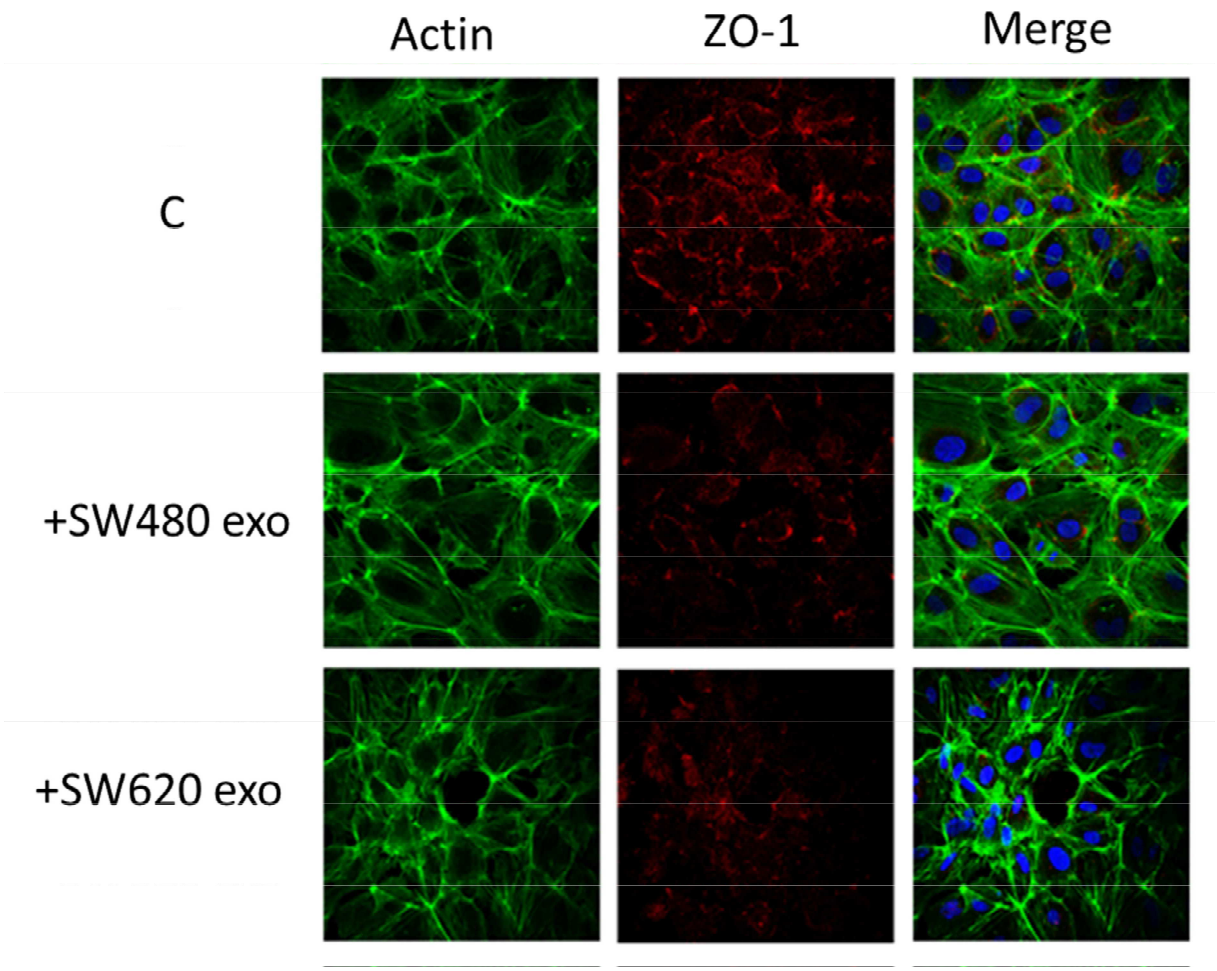

Fig. 28: SW620 exosomes induce a delocalization of ZO-1 (red), after 6 hours of treatment, in comparison to the control and HUVECs treated with SW480 exosomes. HUVECs, treated with 20 µg/ml of exosomes or untreated, are stained with actin green (green), nuclear counterstaining are performed using Hoescht (blue).

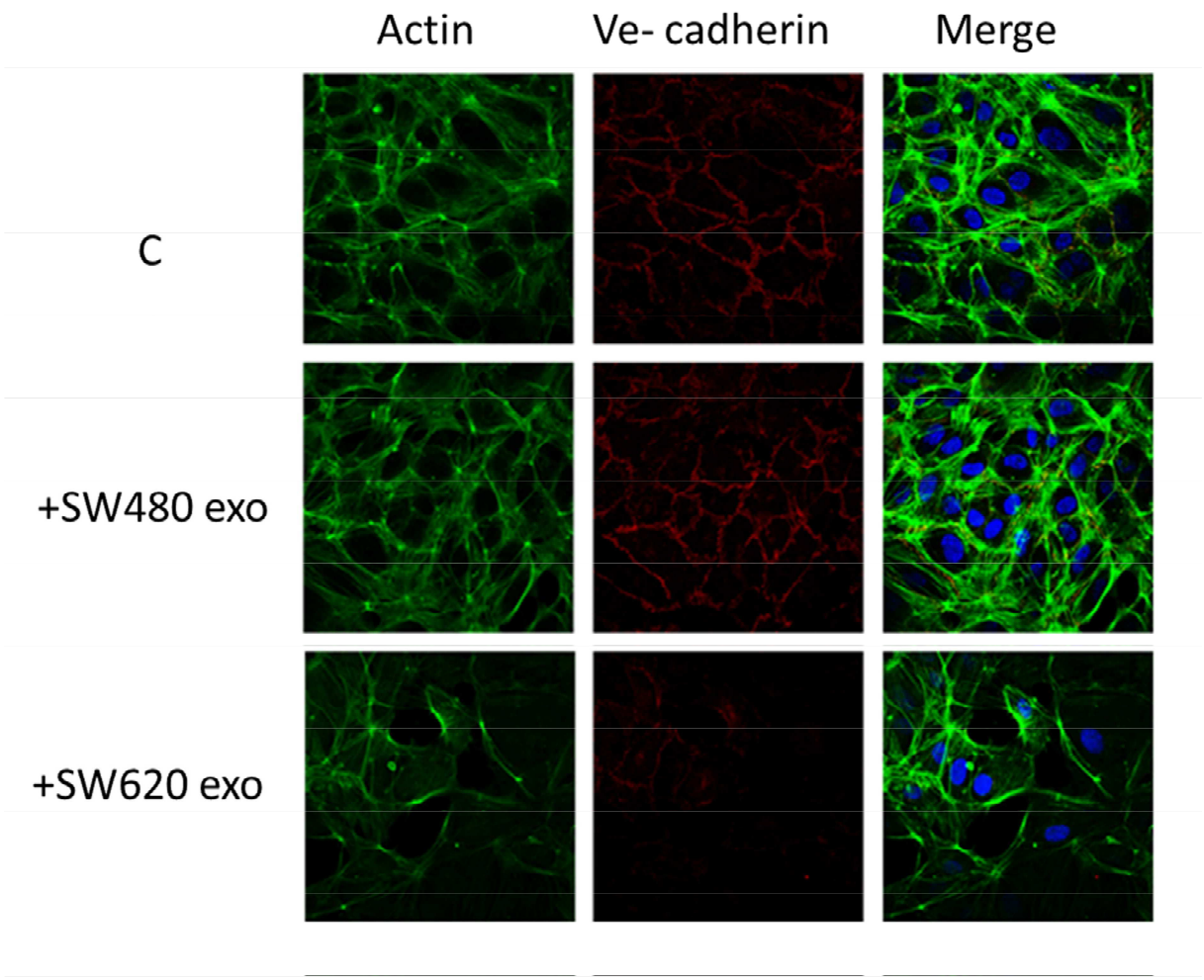

Fig. 29: SW620 exosomes induce a delocalization of Ve-cadherin (red), after 6 hours of treatment, in comparison to the control and HUVECs treatedt with SW480 exosomes. HUVECs, treated with 20 µg/ml of exosomes or untreated, are stained with actin green (green), nuclear counterstaining are performed using Hoescht (blue).

Since VE-cadherin is not sufficient to maintain the endothelial barrier integrity and it is known the role of p120-catenin [97] in interacting with Ve-cadherin on its juxtamembrane domain, leading its- stability at the plasma membrane, we analyze p120-catenin localization, in endothelial cells, after treatments with exosomes. Immunofluorescence approaches in figure 30 show that only endothelial cells treated with exosomes derived from SW620 cells display a delocalization of p120-catenin. This result confirm the role of exosomes derived

from metastatic cell line to increase permeability of endothelial cells, thus inducing a traslocation of Ve-cadherin from the plasma membrane to the cytoplasm.

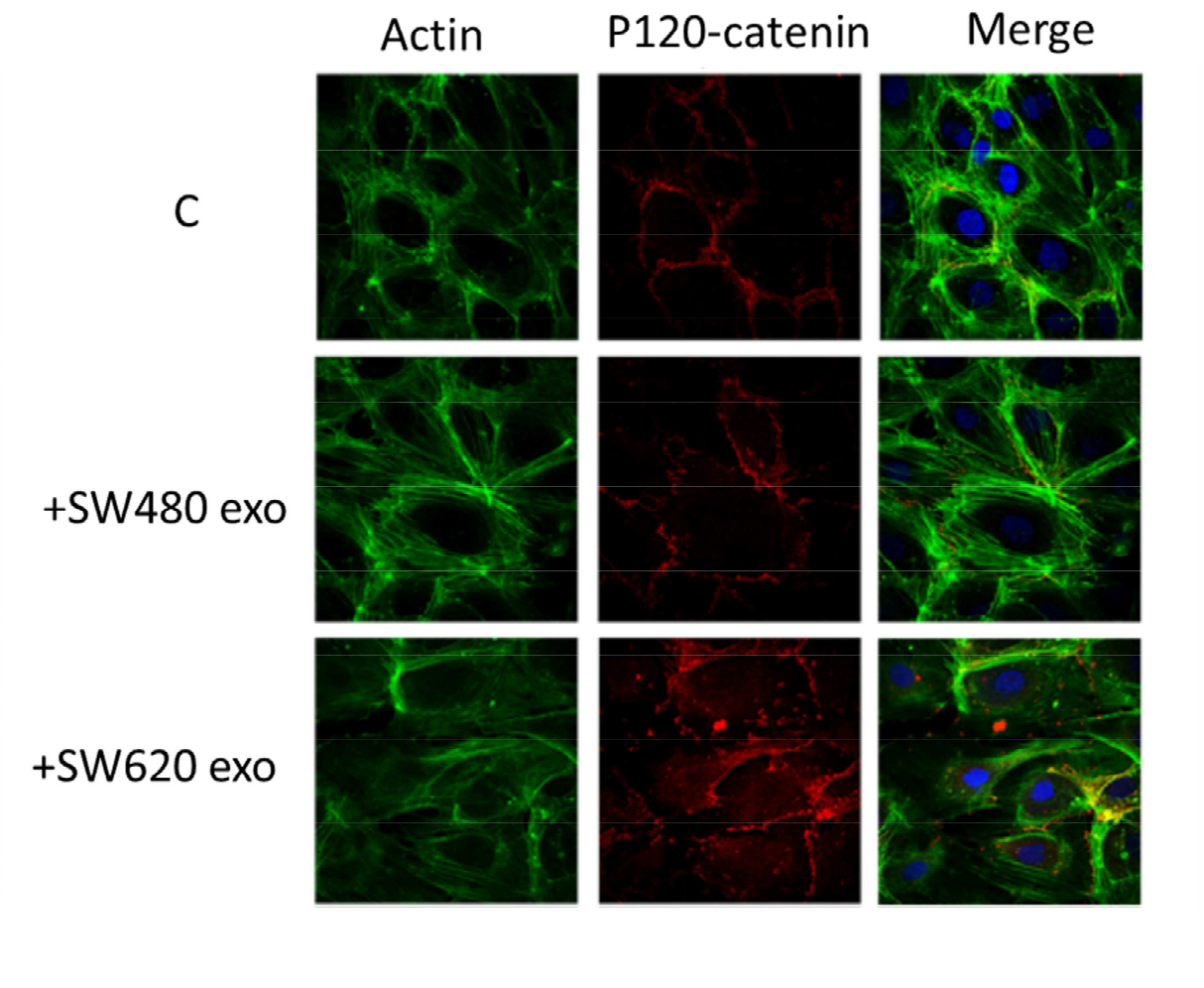

Fig. 30: SW620 exosomes induce a delocalization of p120-catenin (red), after 6 hours of treatment, in comparison to the control and HUVECs treated with SW480 exosomes. HUVECs, treated with 20 µg/ml of exosomes or untreated, are stained with actin green (green), nuclear counterstaining are performed using Hoescht (blue).

SW exosomes promote migration of endothelial cells

Our results show that SW480 and SW620 exosomes added to the upper part of a transwell in which HUVECs are plated, is able to cause, after 6h, an increase of exosome-stimulated endothelial cell migration [Figure 31].

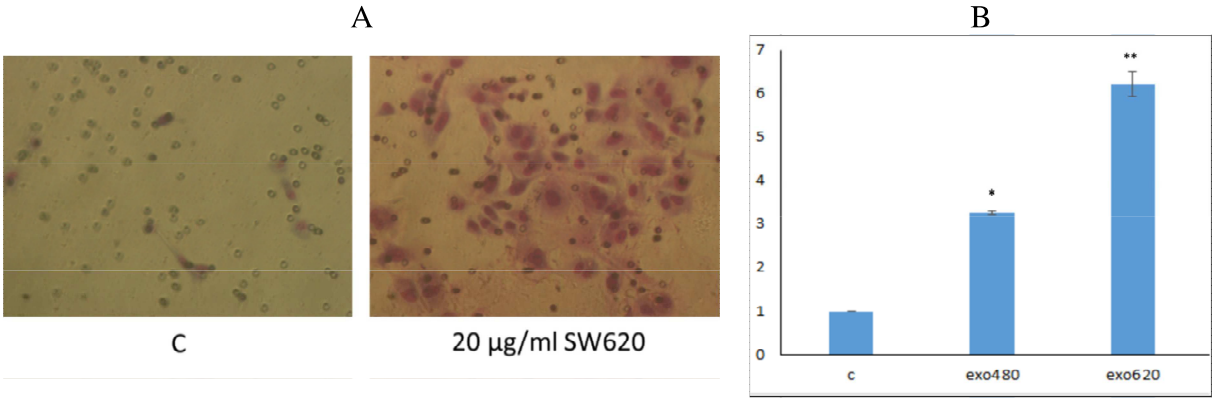

Figure 31: Migration of HUVECs treated with exosomes. A. Representative images of migrated HUVECs observed at contrast phase microscopy. C:control with low serum media B. Migration of HUVECs treated for 6 hours with SW480 and SW620 exosomes. Values are the mean ± SD of 5 fields in three independent experiments *$p < 0.05$, **$p < 0.02$.

SW exosomes promote angiogenesis of endothelial cells

To evaluate the properties of SW exosomes to stimulate angiogenesis, we performed an *in vitro* angiogenesis assay on matrigel As shown in figure 32A-B, the treatment for 6h with SW exosomes induces an endothelial network formation in a dose-dependent manner in HUVECs. These results are confirmed by the measurement of the length of tubular connections [Figure 32B] that showed an increase in cellular projections interconnecting HUVECs after treatment with SW exosomes in a dose-dependent manner. Consistent with the SW620 exosome effects

on modulation of endothelial barrier, the highest SW620 exosome dose is not able to induce tube formation [Figure 32A-B].

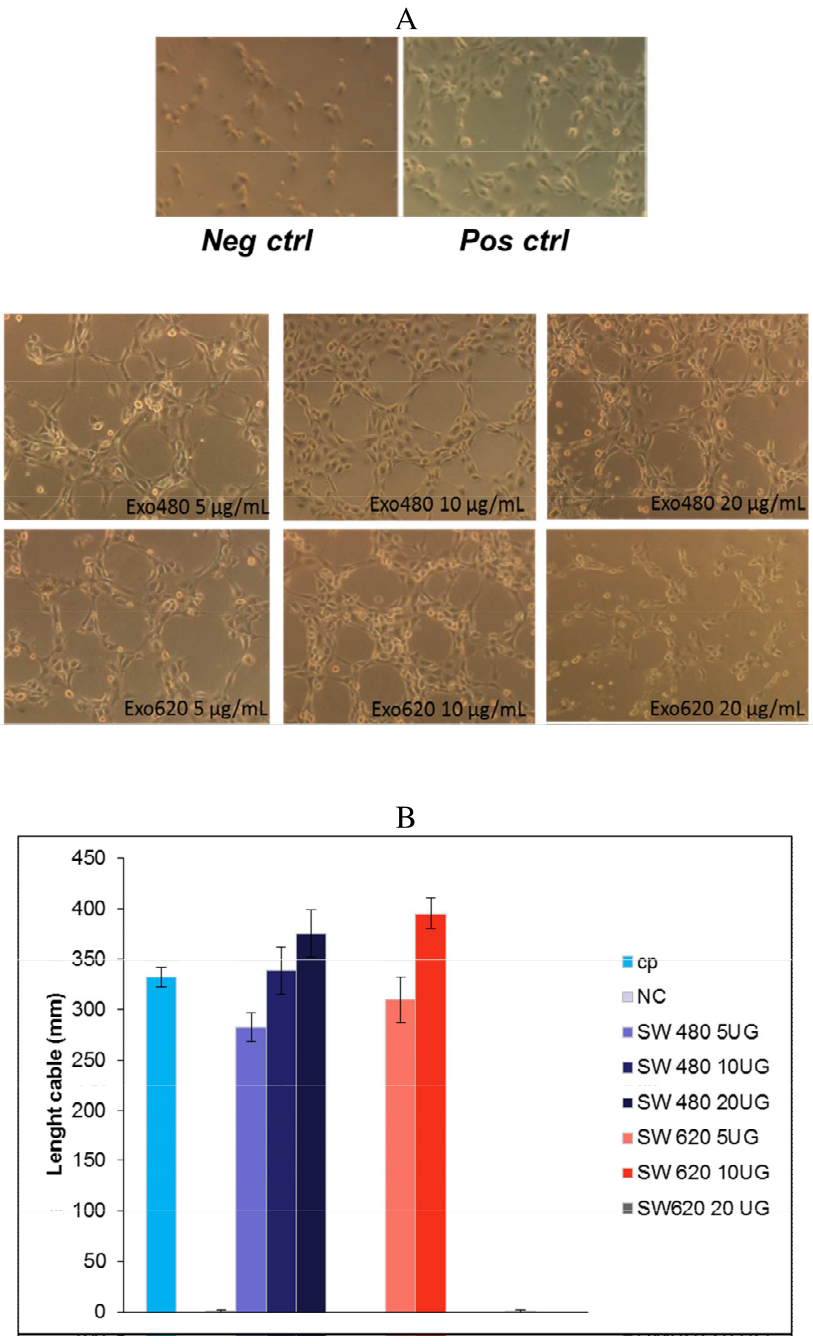

Fig. 32: Exosomes induce an endothelial network formation on matrigel. No tube formation is observed when HUVECs are plated in low-serum medium (neg ctrl) or with 20 µg/ml of SW620 exosomes. The addition to HUVEC cells of increasing doses of SW exosomes causes the formation of capillary-like structures comparable to egm positive control (pos ctrl) condition. A. Phase contrast micrographs showing that exosomes induce an

endothelial network formation on matrigel. B. Measurement of the length of tubular connections. Values are mean of three independent experiments.

SW620 exosomes induce hyperpermeability by Rho A activation

Since data in literature have shown the role of Gtp-Rho A pathway in endothelial barrier maintenance by regulating actin cytoskeleton [96] and since, as previously discussed, SW620 exosomes contain an higher amount of RacGap1 in comparison to SW480 exosomes, our hypothesis is that RacGap1 could represent the possible molecular mediator of HUVECs hyperpermeability.

In order to test whether SW620 exosomes are able to induce the activation of Rho A pathway also in the endothelial system, we examined the level of GTP-Rho A activity. Figure 33 shows that the treatment of HUVECs with SW620 exosomes induces an increase in Rho A activity [Figure 33A], while the level of total protein does not change [Figure 33B].

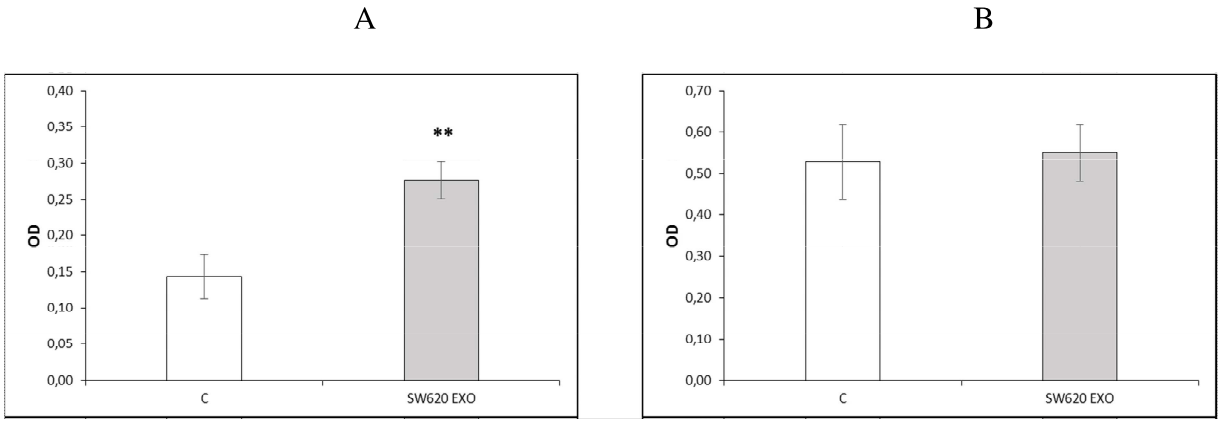

Figure 33: SW620 exosomes activate Rho A pathway. A. After 6 hours of treatment with 20 µg/ml of SW620 exosomes, the level of Rho A activity in HUVECs increases as compared with the basal level. B. In the same condition of treatment the level of total Rho A does not change. Values are the mean of three independent experiments **$p < 0.02$.

This result suggest us the ability of SW620 exosomes to increase the reorganization of cytoskeleton in endothelial cells thus leading to an increase of HUVECs permeability. We believed that this phenotype might be induced by the delocalization of Ve-cadherin from the plasma membrane to cytoplasm.

Conclusions

Tumors are characterized by extensive intratumoral heterogeneity that provides the driving force to evolve and enhance the robustness of cancer. From a therapeutic point of view the dynamic variability of cell populations makes difficult to develop new treatments. So, particularly for more advanced metastatic disease, a better understanding of the molecular mechanisms and of molecules that drive such processes is necessary for the identification of new therapeutic targets. Since the tumor microenvironment was lately recognized as the product of a developing crosstalk among different cells types, it plays an important role in determining the heterogeneity observed within and across tumors. Recently, a number of studies have described exosomes as new players in modulating tumor microenvironment, promoting angiogenesis and tumor progression. In this work, in the context of tumor heterogeneity, we show that exosomes, derived from metastatic SW620 cells, are not only simply vehicles, but new actors between more and less aggressive colon cancer cells. Specifically, they induce a mesenchymal-amoeboid transition in SW480 fibroblast-like cells, thus leading to a higher migratory, invasive and adhesive capability to endothelial cells. Moreover, we showed an increased permeability of HUVEC monolayer after treatment with SW620 exosomes thus suggesting a possible reorganization of junctional component. In addition our data indicate that the effects observed in both cell types are mediated by a protein involved in cytoskeletal remodeling, Rho A, whose activation is induced by SW620 exosomes. Moreover, comparative proteomic analysis strongly confirm our hypothesis showing an enrichment in SW620 exosomes of RacGap1, known activator of Rho A. In conclusion we demonstrated that the exosomes released by metastatic colon cancer cells are able to induce a more aggressive phenotype in less aggressive cells by the activation of Rho A

and modulate the endothelial monolayer permeability driving the metastatic dissemination of cancer cells.

Data presented in this thesis strongly suggest that Rho A can be considered a new target for the development of therapeutics strategies for colon cancer treatment.

References

1. Parkin DM., Pisani P., Ferlay J. Global cancer statistics. CA Cancer J Clin. 1999; 49(1):33-64, 1.
2. Spann SJ., Rozen P., Young GP., Levin B. Colorectal cancer: how big is the problem, why prevent it, and how might it present? In: Rozen P, Young GP, Levin B, Spann SJ, editors. Colorectal Cancer in Clinical Practice. London: Martin Dunitz Ltd; 2002; pp. 1–18.
3. Sengupta N., Gill KA., MacFie TS., Lai CS., Suraweera N., Mcdonald S., Silver A.N. "Management of colorectal cancer: a role for genetics in prevention and treatment?" Pathol Res Pract. 2008; 204(7):469-77.
4. Taylor DP., Burt RW., Williams MS., Haug PJ., Cannon-Albright LA. Population-based family history-specific risks for colorectal cancer: a constellation approach. Gastroenterology. 2010; 138(3):877-85.
5. Kerber RA., Neklason DW., Samowitz WS., Burt RW. Frequency of familial colon cancer and hereditary nonpolyposis colorectal cancer (Lynch syndrome) in a large population database. Fam Cancer. 2005; 4(3):239-44.
6. Hardy RG., Meltzer SJ., Jankowski JA. ABC of colorectal cancer. Molecular basis for risk factors. BMJ. 2000; 321(7265):886-9.
7. Iqbal S., Lenz HJ. Integration of novel agents in the treatment of colorectal cancer. Cancer Chemother Pharmacol. 2004; 54 Suppl 1:S32-9.
8. Potter JD. Colorectal cancer: molecules and populations. J Natl Cancer Inst. 1999; 2; 91(11):916-32.
9. Kinzler KW., Vogelstein B. Lessons from hereditary colorectal cancer. Cell 1996; 87(2):159-70.

10. Fearon ER. Molecular Genetics of Colorectal Cancer. Annu. Rev. Pathol 2011; 6:479–507.

11. Leggett B., Whitehall V. Role of the serrated pathway in colorectal cancer pathogenesis. Gastroenterology 2010; 138:2088-2100.

12. Pino MS., Chung DC. The chromosomal instability pathway in colon cancer. Gastroenterology. 2010;138(6):2059-72.

13. Issa JP. CpG island methylator phenotype in cancer. Nat Rev Cancer 2004; 4: 988-993.

14. Hawkins N, Norrie M., Cheong K., Mokany E., Ku SL., Meagher A., O'Connor T., Ward R. CpG island methylation in sporadic colorectal cancers and its relationship to microsatellite instability. Gastroenterology. 2002; 122(5):1376-87.

15. Setaffy L., Langner C. Microsatellite instability in colorectal cancer: clinicopathological significance. Pol J Pathol 2015; 66 (3): 203-218.

16. Kim IJ., Kang HC., Park JH., Shin Y., Ku JL., Lim SB., Park SY., Jung SY., Kim HK., Park JG. Development and applications of a beta-catenin oligonucleotide microarray: beta-catenin mutations are dominantly found in the proximal colon cancers with microsatellite instability. Clin Cancer Res. 2003; 9(8):2920-5.

17. Liefers GJ., Tollenaar RA. Cancer genetics and their application to individualised medicine. Eur J Cancer. 2002; 38(7):872-9.

18. Toyota M., Ahuja N., Ohe-Toyota M., Herman JG., Baylin SB., Issa JP. CpG island methylator phenotype in colorectal cancer. Proc Natl Acad Sci U S A. 1999; 96(15):8681-6.

19. Marusyk, A., Polyak, K. Tumor heterogeneity: causes and consequences. Biochim Biophys Acta. 2010; 1805(1):105-17.

20. De Sousa E Melo F., Vermeulen L., Fessler E., Medema JP. Cancer heterogeneity—a multifaceted view. EMBO Rep. 2013;14 (8):686-95.

21. Owusu BY., Vaid M., Kaler P., Klampfer L.. Prognostic and Predictive Significance of Stromal Fibroblasts and Macrophages in Colon Cancer. Biomark Cancer. 2015; 7(Suppl 1):29-37.

22. Linnekamp JF., Wang X., Medema JP., Vermeulen L. Colorectal cancer heterogeneity and targeted therapy: a case for molecular disease subtypes. Cancer Res. 2015; 75(2):245-9.

23. De Sousa E Melo .F, Wang X., Jansen M., et al. Poor-prognosis colon cancer is defined by a molecularly distinct subtype and develops from serrated precursor lesions. Nat Med. 2013; 19(5):614-8.

24. Cortes J., Calvo E., Vivancos A., Perez-Garcia J., Recio JA., Seoane J. New approach to cancer therapy based on a molecularly defined cancer classification. J Clin. 2014; 64(1):70-4.

25. Easwaran H., Tsai HC., Baylin SB. Cancer Epigenetics: Tumor Heterogeneity, Plasticity of Stem-like States, and Drug Resistance. Mol Cell. 2014; 54(5):716-27.

26. Fearon ER., Vogelstein B. A genetic model for colorectal tumorigenesis. Cell 1990; 61(5):759-67.

27. Greaves M., Maley CC. Clonal evolution in cancer. Nature. 2012; 481(7381):306-13.

28. Noushmehr H., Weisenberger DJ., Diefes K. et al. Identification of a CpG island methylator phenotype that defines a distinct subgroup of glioma. Cancer Cell. 2010; 17(5):510-22.

29. Lorusso G., Rüegg C. The tumor microenvironment and its contribution to tumor evolution toward metastasis. Histochem Cell Biol 2008 ; 130(6):1091-103.

30. Kucharzewska P., Belting M. Emerging roles of extracellular vesicles in the adaptive response of tumour cells to microenvironmental stress. J Extracell Vesicles, 2013.

31. Vermeulen L. et al. Wnt activity defines colon cancer stem cells and is regulated by the microenvironment. Nat Cell Biol. 2010; 12(5):468-76.

32. Lu J et al. Endothelial cells promote the colorectal cancer stem cell phenotype through a soluble form of Jagged-1. Cancer Cell. 2013; 23(2):171-85.

33. Scheel C., Eaton EN., Li SH., Chaffer CL., Reinhardt F., Kah KJ., Bell G., Guo W., Rubin J., Richardson AL., Weinberg RA. Paracrine and autocrine signals induce and maintain mesenchymal and stem cell states in the breast. Cell. 2011; 145(6):926-40.

34. Valastyan S., Weinberg RA. Tumor Metastasis: Molecular Insights and Evolving Paradigms. Cell. 2011; 147(2):275-92.

35. Paget, S. The distribution of secondary growths in cancer of the breast. Cancer Metastasis Rev. 1989; (2):98-101.

36. Chiang AC., Massagué J. Molecular basis of metastasis. N Engl J Med. 2008; 359(26):2814-23.

37. Friedl, P., Wolf, K. Tumor-cell invasion and migration: diversity and escape mechanism. Nat Rev Cancer. 2003 May;3(5):362-74.

38. Gupta GP., Massagué J. Cancer. Metastasis: Building a Framework. Cell. 2006; 127(4):679-95.

39. Minchenko, A., Salceda, S., Bauer, T. & Caro, J. Hypoxia regulatory elements of the human vascular endothelial growth factor gene. Cell Mol Biol Res. 1994; 40(1):35-9.

40. Staller P., Sulitkova J., Lisztwan J., Moch H., Oakeley EJ., Krek W. Chemokine receptor CXCR4 downregulated by von Hippel-Lindau tumour suppressor pVHL. Nature. 2003; 425(6955):307-11.

41. Sonoshita, M., Aoki M., Fuwa H., Aoki K., Hosogi H., Sakai Y., Hashida H., Takabayashi A., Sasaki M., Robine S., et al. Suppression of colon cancer metastasis by Aes through inhibition of Notch signaling . Cancer Cell. 2011; 19(1):125-37.

42. Joyce J.A., and Pollard J.W. Microenvironmental regulation of metastasis. Nat Rev Cancer. 2009; 9(4):239-52239–252.

43. Demicheli R. Tumour dormancy: findings and hypotheses from clinical research on breast cancer. Semin Cancer Biol. 2001 ; 11(4):297-306.

44. Minciacchi VR., Freeman MR., Di Vizio D. Extracellular Vesicles in Cancer: Exosomes, Microvesicles and the Emerging Role of Large Oncosomes. Semin Cell Dev Biol. 2015; 40:41-51

45. Fontana S., Saieva L., Taverna S. and Alessandro R.. Contribution of proteomics to understanding the role of tumor-derived exosomes in cancer progression: State of the art and new perspectives. Proteomics. 2013; 13(10-11):1581-94.

46. György B et. al. Membrane vesicles, current state emerging role of extracellular vesicles. Cell Mol Life Sci. 2011; 68(16):2667-88.

47. Mathivanan S., Ji H., Simpson RJ. Exosomes: extracellular organelles important in intercellular communication. J Proteomics. 2010; 73(10):1907-20.

48. Simpson RJ., Lim JW., Moritz RL., Mathivanan S. Exosomes: proteomic insights and diagnostic potential. Expert Rev Proteomics. 2009; 6(3):267-83.

49. Raimondo S., Corrado C., Raimondi L., De Leo G., Alessandro R. Role of Extracellular Vesicles in Hematological Malignancies. Biomed Res Int. 2015; 2015:821613.

50. Record M., Subra C., Silvente-Poirot S., Poirot M. Exosomes as intercellular signalosomes and pharmacological effectors. Biochem Pharmacol. 2011; 81(10):1171-82.

51. Runz S., Keller S., Rupp C., Stoeck A., Issa Y., Koensgen D., Mustea A., Sehouli J., Kristiansen G., Altevogt P. Malignant ascites-derived exosomes of ovarian carcinoma patients contain CD24 and EpCAM. Gynecol Oncol. 2007; 107(3):563-71.

52. Mears R., Craven RA., Hanrahan S., Totty N., Upton C., Young SL., Patel P., Selby PJ., Banks RE. Proteomic analysis of melanoma-derived exosomes by two-dimensional polyacrylamide gel electrophoresis and mass spectrometry. Proteomics. 2004; 4(12):4019-31.

53. Luigini et al. Immune surveillance properties of human nk cell-derived exosomes. J Immunol. 2012; 189(6):2833-42.

54. Faure et al. Exosomes are released by cultured cortical neurons. Mol Cell Neurosci. 2006; 31(4):642-8.

55. Yu X., Riley T., Levine AJ. The regulation of the endosomal compartment by p53 the tumor suppressor gene. FEBS J. 2009 ; 276(8):2201-12.

56. Nazarenko I. Rana S., Baumann A., McAlear J., Hellwig A., Trendelenburg M., Lochnit G., Preissner KT., Zoller M. Cell surface tetraspanin Tspan8 contributes to molecular pathways of exosome induced endothelial cell activation. Cancer Res. 2010; 70(4):1668-78.

57. Rana S., Yue S., Stadel D., Zoller M. Toward tailored exosomes: the exosomal tetraspanin web contributes to target cell selection. Int J Biochem Cell Biol. 2012; 44(9):1574-84.

58. Clayton A., Turkes A., Dewitt S., Steadman R., Mason MD., Hallett MB. Adhesion and signaling by B cell-derived exosomes: the role of integrins. FASEB J. 2004; 18(9):977-9.

59. Feng D., Zhao WL., Ye YY., Bai XC., Liu RQ., Chang LF., Zhou Q., Sui SF. Cellular internalization of exosomes occurs through phagocytosis. Traffic. 2010; 11(5):675-87.

60. Mathivanan S., Lim JW., Tauro BJ., Ji H., Moritz RL., Simpson RJ. Proteomics analysis of A33 immunoaffinity-purified exosomes released from the human colon tumor cell line LIM1215 reveals a tissue-specific protein signature. Mol Cell Proteomics. 2010; 9(2):197-208.

61. Simons M., Raposo G. Exosomes–vesicular carriers for intercellular communication. Curr Opin Cell Biol. 2009; 21(4):575-81.

62. Luga V.; Zhang L.; Viloria-Petit AM.; Ognunjimi AA.; Inanlou MR.; Chiu E.; Buchanan M.; Hosein AN.; Basik M.; Wrana J.L. Exosomes mediate stromal

mobilization of autocrine wnt-pcp signaling in breast cancer cell migration. Cell. 2012; 151(7):1542-56.

63. Al-Nedawi K., Meehan B., Micallef J., Lhotak V., May L., Guha A., Rak J. Intercellular transfer of the oncogenic receptor EGFRvIII by microvesicles derived from tumour cells. Nat Cell Biol. 2008; 10(5):619-24.

64. Khan S., Aspe JR., Asumen MG., Almaguel F., Odumosu O., Acevedo-Martinez S., De Leon M., Langridge WH., Wall NR.S. Extracellular, cell-permeable survivin inhibits apoptosis while promoting proliferative and metastatic potential. Br J Cancer. 2009; 100(7):1073-86.

65. Demory Beckler M., Higginbotham JN., Franklin JL., Ham AJ., Halvey PJ., Imasuen IE., Whitwell C., Li M., Liebler DC., Coffey RJ. Proteomic analysis of exosomes from mutant KRAS colon cancer cells identifies intercellular transfer of mutant KRAS. Mol Cell Proteomics. 2013; 12(2):343-55.

66. Zomer A., Vendrig T., Hopmans ES., van Eijndhoven M., Middeldorp JM., Pegtel DM. Exosomes: fit to deliver small RNA. Commun Integr Biol. 2010; 3(5):447-50.

67. Valadi H., Ekström K., Bossios A., Sjöstrand M., Lee JJ., Lötvall JO. Exosome mediated transfer of mRNAs and microRNAs is a novel mechanism of genetic exchange between cells. Nat Cell Biol. 2007; 9(6):654-9.

68. Corcoran C., Rani S., O'Brien K., O'Neill A., Prencipe M., Sheikh R., Webb G., McDermott R., Watson W., Crown J., O'Driscoll L. Docetaxel-Resistance in Prostate Cancer: Evaluating Associated Phenotypic Changes and Potential for Resistance Transfer via Exosomes. PLoS One. 2012; 7(12):e50999.

69. Jung T., Castellana D., Klingbeil P., Cuesta Hernandez I., Vitacolonna M., Orlicky DJ., Roffler SR., Brodt P., Zoller M. CD44v6 dependence of premetastatic niche preparation by exosomes. Neoplasia. 2009; 11(10):1093-105.

70. Peinado H., Aleckovic M., Lavotshkin S., Matei I., Costa-Silva B., Moreno-Bueno G., Hergueta- Redondo M., Williams C., Garcia-Santos G., Ghajar C., et al. Melanoma exosomes educate bone marrow progenitor cells toward a pro-metastatic phenotype through MET. Nat Med. 2012; 18(6):883-91.

71. Lamparski HG., Metha-Damani A., Yao JY., Patel S., Hsu DH., Ruegg C., Le Pecq JB. Production and characterization of clinical grade exosomes derved from dendritic cells. J Immunol Methods. 2002; 270(2):211-26.

72. Choi DS., Choi DY., Hong BS., Jang SC., Kim DK., Lee J., Kim YK., Kim KP. and Gho YS. Quantitative proteomics of extracellular vesicles derived from human primary and metastatic colorectal cancer cells. Journal of extracellular vesicles. J Extracell Vesicles. 2012.

73. Noto R., Santangelo MG., Ricagno S., Mangione MR., Levantino M., Pezzullo M., Martorana V., Cupane A., Bolognesi M. and Manno M. The tempered polymerization of human neuroserpin. PLoS One. PLoS One. 2012; 7(3):e32444.

74. Taverna S., Flugy A., Saieva L., Kohn EC., Santoro A., Meraviglia S., De Leo G. and Alessandro R. Role of exosomes released by chronic myelogenous leukemia cells in angiogenesis. Int J Cancer. 2012; 130(9):2033-43.

75. Taverna S., Flugy A., Colomba P., Barranca M., De Leo G., Alessandro R. Effects of Parietaria judaica pollen extract on human microvascular endothelial cells. Biochem Biophys Res Commun. 2008; 372(4):644-9.

76. Hager MH., Morley S., Bielenberg DR., Gao S., Morello M., Holcomb IN., Liu W., Mouneimne G., Demichelis F., Kim J., Solomon KR., Adam RM., Isaacs WB., Higgs HN., Vessella RL., Di Vizio D., Freeman. DIAPH3 governs the cellular transition to the amoeboid tumour phenotype. EMBO Mol Med. 2012; 4(8):743-60.

77. Morello M., Minciacchi VR., de Candia P., Yang J., Posadas E., Kim H., Griffiths D., Bhowmick N., Chung LW., Gandellini P., Freeman MR., Demichelis F. and Di Vizio D.

Large oncosomes mediate intercellular transfer of functional microRNA. Cell Cycle. 2013; 12(22):3526-36.

78. Sui Y., Wu F., Lv J., Li H., Li X., Du Z., Sun M1., Zheng Y., Yang L., Zhong L1., Zhang X., Zhang G. Identification of the Novel TMEM16A Inhibitor Dehydroandrographolide and Its Anticancer Activity on SW620 Cells. PLoS One. 2015; 10(12):e0144715.

79. Kohn EC., Alessandro R., Spoonster J., Wersto RP., Liotta LA. Angiogenesis: role of calcium-mediated signal transduction. Proc Natl Acad Sci U S A. 1995; 92(5):1307-11.

80. Rodriguez LG., Wu X., Guan JL. Wound-healing assay. Methods Mol Biol. 2005;294:23-9.

81. Principe S., Jones EE., Kim Y., Sinha A., Nyalwidhe JO., Brooks J., Semmes OJ., Troyer DA., Lance RS., Kislinger T., Drake RR. In-depth proteomic analyses of exosomes isolated from expressed prostatic secretions in urine. Proteomics, 2013; 13(10-11):1667-71.

82. Ridgway LD., Wetzel MD., Marchetti D. Modulation of GEF-H1 Induced Signaling by Heparanase in Brain Metastatic Melanoma Cells. J Cell Biochem. 2010; 111(5):1299-309.

83. Imaoka H., Toiyama Y., Saigusa S., Kawamura M. et al. RacGAP1 expression, increasing tumor malignant potential, as a predictive biomarker for lymph node metastasis and poor prognosis in colorectal cancer. Carcinogenesis. 2015; 36(3):346-54.

84. Guillaume J., Green DM., Bridgewater RE., et al. RCP-driven α5β1 recycling suppresses Rac and promotes RhoA activity via the RacGAP1–IQGAP1 complexJ. Cell Biol. Vol. 202 No. **6** 917–935.

85. Zhang P., Bai H., Fu C., Chen F., et al. RacGAP1-driven focal adhesion formation promotes melanoma transendothelial migration through mediating adherens junction

disassembly. Biochemical and Biophysical Research Communications, 2015; 459 (1) 1-9.

86. Rao D., Kimler BF., Notnick WB., Davis MK., Fan F.., Tawfik O. Transgelin: a potentially useful diagnostic marker differentially expressed in triple-negative and non-triple-negative breast cancers. Human Pathology 2015; 46 (6) 876-83.

87. Liu J, Huang W., Ren C., et al. Flotillin-2 promotes metastasis of nasopharyngeal carcinoma by activating NF-κB and PI3K/Akt3 signaling pathways. Sci-Rep, 2015; 24;5:11614.

88. Garibay-Cerdenares OL., Hernández-Ramírez V., Osorio-Trujillo JC., Gallardo-Rincón D. and Talamás-Rohana P.. Haptoglobin and CCR2 receptor expression in ovarian cancer cells that were exposed to ascetic fluid: Exploring a new role of haptoglobin in the tumoral microenvironment. Cell Adhesion and Migration 2015; 9:5, 394-405.

89. Desiniotis A. and Kyprionou N. Significance of talinin cancer progression and metastasis. Int Rev Cell Mol Biol. 2011; 289:117-47.

90. Sebbagh M., Renvoize C., Hamelin J., Riche N., Bertoglio J., and Breard J. Caspase-3-mediated cleavage of ROCK I induces MLC phosphorylation and apoptotic membrane blebbing. Nature Cell Biol.2001; 3, 346-352.

91. Alexandrova A Y. Plasticity of Tumor Cell Migration: Acquisition of New Properties or Return to the Past?. Biokhimiya, 2014; Vol. 79, No. 9, pp. 1169-1187.

92. Yoshida K., and Soldati T. Dissection of amoeboid movement into two mechanically distinct modes. J. Cell Sci., 2006; 119, 3833-3844.

93. Maugis B., Brugues J., Nassoy P., Guillen N., Sens P. and Amblard F. Dynamic instability of the intra-intracellular pressure drives bleb-based motility. J. Cell Sci, 2010; 123, 3884-3892.

94. Minciacchi V R., You S., Spinelli C., Morley S., et al. Large oncosomes contain distinct protein cargo and represent a separate functional class of tumor-derived extracellular vesicles. Oncotarget, 2015; Vol. 6, No. 13.

95. Extracellular Vesicles in Cancer: Exosomes, Microvesicles and the Emerging Role of Large Oncosomes. Minciacchi VR., Freeman MR., Di Vizio D. Seminars in Cell & Developmental Biology, 2015; 41–51.

96. Hager M H., Morley S., Bielenberg D R., Gao S., Morello M., Holcomb I N., Liu W., Mouneimne G., Demichelis F., Kim J., Solomon K R., Adam R M., Isaacs W B, Higgs H N., Vessella R L., Di Vizio D., et al. DIAPH3 governs the cellular transition to the amoeboid tumour phenotype. EMBO Mol Med. 2012; 4(8):743-760.

97. Huang Y., Tan Q., Chen R., Cao B., Li W. Sevoflurane prevents lipopolysaccharide-induced barrier dysfunction in human lung microvascular endothelial cells: Rho-mediated alterations of VE-cadherin. Biochem Biophys Res Comm.2015; 468(1-2):119-24.

98. Gavar J. Endothelial permeability and VE-cadherin A wacky comradeship. Cell Adhesion & Migration. 2013; 7:6, 455–461.

99. Setyawati MI., Tay C Y., et al.Titanium dioxide nanomaterials cause endothelial cell leakiness by disrupting the homophilic interaction of VE–cadherin. Nature communications. 2013;4:1673.